Entanglement production in coupled chaotic systems: Case of the kicked tops

Jayendra N. Bandyopadhyay* and Arul Lakshminarayan[†,‡]
Physical Research Laboratory, Navrangpura, Ahmedabad 380009, India
(Received 21 July 2003; published 14 January 2004)

Entanglement production in coupled chaotic systems is studied with the help of kicked tops. Deriving the correct classical map, we have used the reduced Husimi function, the Husimi function of the reduced density matrix, to visualize the possible behaviors of a wave packet. We have studied a phase-space based measure of the complexity of a state and used random matrix theory (RMT) to model the strongly chaotic cases. Extensive numerical studies have been done for the entanglement production in coupled kicked tops corresponding to different underlying classical dynamics and different coupling strengths. An approximate formula, based on RMT, is derived for the entanglement production in coupled strongly chaotic systems. This formula, applicable for arbitrary coupling strengths and also valid for long time, complements and extends significantly recent perturbation theories for strongly chaotic weakly coupled systems.

DOI: 10.1103/PhysRevE.69.016201 PACS number(s): 05.45.Mt, 03.65.Ud, 03.67.−a

I. INTRODUCTION

A quantum mechanical system, which consists of at least two interacting subsystems, has an unique property called 'entanglement' [1]. This property is unique in the sense that even if we know the exact state of the system, it is in general not possible to assign any pure state to the subsystems. Entanglement is a nonclassical correlation among the subsystems which exists even between spatially well separated subsystems [2]. This unique property of a quantum system has been characterized as a quantum resource for quantum information theory and quantum computation [3]. Moreover, quantum entanglement has also been studied extensively from the decoherence point of view. It has been argued that a quantum system in the presence of an ''environment'' can loose its coherence and behave more like a classical system [4].

A quantum computer is a collection of many interacting particles. Such a many-particle structure may be prone to problems of decoherence and chaos. Decoherence can create some errors in the operation of a quantum computer, however, these errors, in principle, can be removed by quantum error correcting codes [3]. On the other hand, the problem due to chaos has recently attracted some attention. It has been shown that residual, uncontrolled interaction between the particles might induce quantum chaos in the quantum computer if the interaction strength crosses certain critical limits and consequently, it may destroy the operational condition of the quantum computer [5]. Besides quantum chaos can also emerge during the implementation of some quantum algorithms [6]. Obviously, a quantum algorithm which simulates a quantum chaotic system is by definition a unitary operation showing quantum chaos [7]. However, it has been shown that well-known algorithms, such as Grover's search algorithm and the quantum Fourier transform algorithm give rise to some unusual combination of quantum signatures of chaos and of integrability [6]. The error due to the presence of chaos in a quantum computer can also be corrected by error correcting codes, but the presence of chaos enhances the complexity and hence much more error correction is needed [8]. Therefore, the knowledge of the presence and effects of chaos in a quantum computer is necessary to implement proper error correcting codes. Very recently, the behavior of quantum entanglement during the operation of an efficient algorithm for quantum chaos have been studied [9]. However, here we are interested at a more basic level to study the effect of the underlying classical dynamics on entanglement production.

Recently, several studies have explored this question [10–18]. The first one studied the entanglement production in an *N*-atom Jaynes-Cummings model [10], and they found that the entanglement rate was considerably enhanced if the initial wave packet was placed in a chaotic region. They also argued that their results support an earlier conjecture which predicted that the entanglement production in a chaotic system, coupled to an environment, would be more than the regular system [19]. According to that conjecture, the entanglement production rate would be higher for a chaotic system coupled to an environment. For the *N*-atom Jaynes-Cummings model, each atomic subsystem plays the role of an environment for the other. Later, it has been shown that large entanglement production rate is not the hallmark of a nonintegrable system [11]. Even in the integrable *N*-atom Jaynes-Cummings model some special initial coherent states exhibit strikingly similar entanglement production as corresponding to the chaotic case [12].

In another paper, the entanglement production rate has been related to the classical Lyapunov exponents with the help of a coupled kicked tops model [13]. They also justified their findings on the basis of the above mentioned conjecture [19]. However, the classical limit of the coupled kicked tops derived in this rather well-quoted work is incorrect, in fact it is not even canonical. However, they consider very weakly coupled tops and therefore their conclusions turn out to be qualitatively valid. In other work, one of us studied the entanglement in coupled standard maps and found that en-

*Electronic address: jayendra@prl.ernet.in
[†]Present address: Department of Physics, Indian Institute of Technology, Madras, Chennai 600036, India.
[‡]Electronic address: arul@physics.iitm.ac.in

tanglement increased with coupling strength, but after a certain magnitude of coupling strength corresponding to the emergence of complete chaos, the entanglement saturated [14]. Similar saturation of entanglement was also observed for a time evolving state, which was initially unentangled. This saturation value depended on the Hilbert space dimension of the participating subsystems, and was less than its maximum possible value. It was also pointed out that in analogy with environment induced decoherence, the reduced density matrices (RDMs) corresponding to subsystems of fully chaotic systems are diagonally dominant.

Later, we derived the saturation value of the entanglement using random matrix theory [15]. Moreover, we presented a universal distribution of the eigenvalues of the RDM's, and demonstrated that this distribution is realized in quantized chaotic systems by using the model of coupled kicked tops. Subsequently, an analytical explanation for the entanglement production, based on perturbation theory, has been given for two weakly coupled strongly chaotic systems [16]. The authors also found that increase in the strength of chaos does not enhance the entanglement production rate for the case of weakly coupled, *strongly* chaotic, subsystems. In a recent work, entropy production in subsystems has been examined as a dynamical criterion for quantum chaos [17]. It has been observed that the power spectrum of the entropy production gets progressively broad banded with a progressive transition from regular to chaotic systems. More recently, entanglement production has been investigated in a class of quantum Baker's map [18]. They also found that, in general, the quantum Baker's map is a good dynamical system to generate entanglement.

Besides these studies of entanglement production and decoherence in coupled chaotic systems, extensive studies have been done on decoherence of chaotic systems that are coupled to an environment. These studies were mainly motivated by the fact that decoherence induces a transition from quantum to classicallike behavior and therefore, this decoherent approach can be utilized in a more straightforward way to restore the correspondence between a quantum chaotic system and its classical counterpart [19]. Irreversibility is the price of this decoherent model for the restoration of quantum-classical correspondence in a quantum system. This irreversibility causes entropy production in the system. It has been conjectured, as already mentioned, that this entropy, grows linearly in time with a fixed rate determined by the Lyapunov exponents.

This conjecture has been tested for several model open quantum chaotic systems. It has been shown that the entropy production rate, as a function of time, in a quartic double well with harmonic driving coupled to a sea of harmonic oscillators has at least two distinct regimes [20]. For short times this rate is proportional to the system-environment coupling strength, and for longer times there is a regime where this rate is determined by the Lyapunov exponent. In another work, the entropy production in Baker's map and Harper's map coupled to a diffusive environment is studied [21]. A regime was found to exist where the entropy production rate is determined by the system's dynamical properties such as Lyapunov exponents, folding rates, etc., and moreover, in this regime the entropy production rate becomes independent of the system-environment coupling strength. Similar results are also reported in Refs. [22,23]. In other work evidence has been presented that the decoherence rate (or entropy production rate) of a quantum system coupled to an environment is governed by a quantity which is a measure of both the increasingly detailed structure of the quantum distributions (Wigner function) and classical phase-space distributions [24].

Very recently, it has been reported that, in open quantum systems, there exists a universal scaling among the parameters (effective Planck's constant, measure of the coupling strength between system and environment, classical Lyapunov exponents) on which the quantum-classical transition of that system depends [25]. In another direction, decoherence has been discussed in an open system coupled to a nonlinear environment with finite degrees of freedom [26]. It was found that even though the environment is finite dimensional, the strong nonlinearity of it can destroy the quantum coherence. Hence there is a possibility to utilize this finite dimensional chaotic system as a model of environment, instead of infinite dimensional heat bath. The above possibility has also been discussed in a recent work [27]. Naturally, this approach is closely linked to studies like the present one on the coupled kicked tops.

We have discussed two different approaches in the study of entanglement production and decoherence in chaotic systems. First approach was to study the entanglement production and decoherence in coupled chaotic systems by performing exact numerical calculation or using some model based on random matrix theory (RMT) and perturbation theory. The second approach was mainly based on approximate master equations. In this paper, following the first approach, we have studied entanglement production in coupled kicked tops. We have considered the entanglement production for both chaotic and regular cases. Besides considering the effect of different kind of classical dynamics on quantum entanglement, we have also considered the effect of different coupling strengths on entanglement production. We have extensively studied a measure of the complexity of the time evolving state, based on the second moment of the Husimi function of that state, corresponding to both single and coupled tops. Using RMT, we have explained the behaviors of this measure for strongly chaotic cases. We have then derived an analytical formula for the entanglement production in coupled strongly chaotic systems using RMT. This formula is applicable for any coupling strength and it also valid for sufficiently long time.

This paper consists of six sections. In Sec. II we have discussed the quantum and classical properties of coupled kicked tops. We have presented the correct classical map of the coupled kicked tops. We have discussed the initial states used and have defined the measures of entanglement used here. Finally, we have concluded this section by discussing a method to visualize the wave packet of a coupled system on the phase space of a subsystem. In Sec. III we have considered a recently proposed method to measure the complexity of a quantum state. Using this method, we have defined a measure which quantifies the fraction of the total number of

Planck cells occupied by the Husimi function of a given state, roughly speaking the amount of ''phase space'' that is filled by the Husimi.

The Hilbert space dimension is the number of Planck cells, each of volume h^d, which fit into the total phase-space volume. In one dimension, $d=1$, then N = phase-space area/h. The above mentioned measure of the complexity of quantum states is also approximately equal to the fraction of the Hilbert space occupied by the given state. We have observed for the single top that a typical time evolving state can occupy half of the total number of the Planck cells, and this happens only for the strongly chaotic cases. Whereas for a highly chaotic top coupled strongly to another such top, the above measure, now for the reduced density matrix of each top, has reached a value very close to unity. We explain the behavior of this measure, using RMT, for the strongly chaotic cases. For nonchaotic and mixed cases, the time evolving state occupies lesser number of Planck cells and is reflected in smaller values of this measure.

In Sec. IV, we have presented the numerical results on the entanglement production. In Sec. V, we have derived an approximate formula, based on RMT, to explain the entanglement production in coupled strongly chaotic systems. Finally, we summarize in Sec. VI.

II. COUPLED KICKED TOPS

A. Quantum top

The single kicked top is a system, characterized by an angular momentum vector $\mathbf{J}=(J_x,J_y,J_z)$, where these components obey the usual angular momentum algebra. We set Planck's constant to unity. The dynamics of the top is governed by the Hamiltonian [28]

$$H(t)=pJ_y+\frac{k}{2j}J_z^2\sum_{n=-\infty}^{+\infty}\delta(t-n). \tag{1}$$

The first term describes free precession of the top around y axis with angular frequency p, and the second term is due to periodic δ-function kicks. Each such kick results in a torsion about z axis by an angle proportional to J_z, and the proportionality factor is a dimensionless constant $k/2j$. Now, to study the entanglement between two tops, we consider the Hamiltonian of the coupled kicked tops which can be written, following Ref. [13], as

$$\mathcal{H}(t)=H_1(t)+H_2(t)+H_{12}(t), \tag{2}$$

where

$$H_i(t)\equiv p_iJ_{y_i}+\frac{k_i}{2j}J_{z_i}^2\sum_n\delta(t-n), \tag{3}$$

$$H_{12}(t)\equiv\frac{\epsilon}{j}J_{z_1}J_{z_2}\sum_n\delta(t-n), \tag{4}$$

where $i=1,2$. Here $H_i(t)$'s are the Hamiltonians of the individual tops, and $H_{12}(t)$ is the coupling between the tops using spin-spin interaction term with a coupling strength of ϵ/j. All these angular momentum operators obey standard commutation relations. For the rest of the paper we will only concentrate to the case $p_1=p_2=\pi/2$. This special choice of the angular frequencies will simplify both the quantum and classical maps. Since J_i^2 and J_{z_i}'s are four mutually commuting operators, the simultaneous eigenvectors of these operators we take as our basis. In general, this basis is denoted by $|j_1,m_1;j_2,m_2\rangle=|j_1,m_1\rangle\otimes|j_2,m_2\rangle$, where $J_i^2|j_i,m_i\rangle=j_i(j_i+1)|j_i,m_i\rangle$ and $J_{z_i}|j_i,m_i\rangle=m_i|j_i,m_i\rangle$. The individual top angular momentums, j_1 and j_2, could in general be different.

The time evolution operator, defined in between two consecutive kicks, corresponding to this coupled Hamiltonian is given by

$$U_T=U_{12}^{\epsilon}(U_1\otimes U_2)=U_{12}^{\epsilon}[(U_1^kU_1^f\otimes(U_2^kU_2^f)], \tag{5}$$

where the different terms are given by,

$$U_i^f\equiv\exp\left(-i\frac{\pi}{2}J_{y_i}\right),\quad U_i^k\equiv\exp\left(-i\frac{k}{2j}J_{z_i}^2\right),$$

$$U_{12}^{\epsilon}\equiv\exp\left(-i\frac{\epsilon}{j}J_{z_1}J_{z_2}\right), \tag{6}$$

and as usual $i=1,2$.

B. Classical top

The corresponding classical map of the coupled kicked tops discussed above can be obtained from the quantum description with the Heisenberg picture in which the angular momentum operators evolve as

$$\mathbf{J}(n+1)=U_T^{\dagger}\mathbf{J}(n)U_T. \tag{7}$$

Now we have to determine the explicit form of this angular momentum evolution equation for each component of the angular momentum. Here we present the time evolution of J_{x_1} (see Appendix A):

$$J'_{x_1}\equiv U_T^{\dagger}J_{x_1}U_T=\frac{1}{2}(J_{z_1}+iJ_{y_1})\exp\left[i\frac{k}{j}\left(-J_{x_1}+\frac{1}{2}\right)\right]$$
$$\otimes\exp\left(-i\frac{\epsilon}{j}J_{x_2}\right)+\frac{1}{2}\exp\left[-i\frac{k}{j}\left(-J_{x_1}+\frac{1}{2}\right)\right](J_{z_1}-iJ_{y_1})$$
$$\otimes\exp\left(i\frac{\epsilon}{j}J_{x_2}\right). \tag{8}$$

The above expression differs from the coupled tops map presented in a previous publication [13]. First, J'_{x_1} is now really a Hermitian operator. Second, the terms which arise in the above expression due to the interaction, contain J_{x_2} operator instead of J_{y_2}. We proceed by rescaling the angular momentum operator as $(X_i,Y_i,Z_i)\equiv(J_{x_i},J_{y_i},J_{z_i})/j$, for $i=1,2$. Components of this rescaled angular momentum vector satisfy the commutation relations, $[X_i,Y_i]=iZ_i/j$,$[Y_i,Z_i]=iX_i/j$ and $[Z_i,X_i]=iY_i/j$. Therefore, in $j\to\infty$ limit, com-

ponents of this rescaled angular momentum vector will commute and become classical *c*-number variables. Consequently, in this large-j limit, we obtain the classical map corresponding to coupled kicked tops as

$$X_1' = Z_1 \cos\Delta_{12} + Y_1 \sin\Delta_{12}, \tag{9a}$$

$$Y_1' = -Z_1 \sin\Delta_{12} + Y_1 \cos\Delta_{12}, \tag{9b}$$

$$Z_1' = -X_1, \tag{9c}$$

$$X_2' = Z_2 \cos\Delta_{21} + Y_2 \sin\Delta_{21}, \tag{9d}$$

$$Y_2' = -Z_2 \sin\Delta_{21} + Y_2 \cos\Delta_{21}, \tag{9e}$$

$$Z_2' = -X_2, \tag{9f}$$

where

$$\Delta_{12} \equiv kX_1 + \epsilon X_2 \quad \text{and} \quad \Delta_{21} \equiv kX_2 + \epsilon X_1. \tag{10}$$

The difference between the map presented above and the one which was derived in Ref. [13] lies in the form of the angles Δ_{12} and Δ_{21}. However, these differences are very important. The above map is canonical. It satisfies all Poisson bracket relations such as $\{X_i', Y_i'\} = Z_i'$, $\{Y_i', Z_i'\} = X_i'$ and $\{Z_i', X_i'\} = Y_i'$, where $i = 1,2$, and Poisson brackets of any two dynamical variables corresponding to different tops are equal to zero. In contrast, the classical map presented in Ref. [13] satisfies the first three Poisson bracket relations, but the Poisson brackets of any two dynamical variables corresponding to different tops are nonzero and they are proportional to the coupling strength ϵ, implying that the map is canonical only in the uncoupled limit. Moreover, this earlier publication relates the entanglement rate to the sum of the positive Lyapunov exponents, which were actually determined using the incorrect classical map. However, they considered very weak coupling ($\epsilon = 10^{-3}$) among the tops and therefore the error in the calculation of the Lyapunov exponents was very small, these being practically those of the uncoupled tops. Hence we believe that the main conclusions presented in that paper are still valid.

In the limit $\epsilon \to 0$, we will arrive at the map corresponding to the single kicked top, whose Hamiltonian is given in Eq. (1), and that map is given by

$$X' = Z \cos kX + Y \sin kX, \tag{11a}$$

$$Y' = -Z \sin kX + Y \cos kX, \tag{11b}$$

$$Z' = -X. \tag{11c}$$

The classical dynamics of the single top have been studied extensively in Refs. [28,29] and is a well studied model of quantum chaos. From the above expressions, it is clear that the variables (X,Y,Z) lie on the sphere of radius unity, i.e., $X^2 + Y^2 + Z^2 = 1$. This constraint on the dynamical variables restricted the classical motion to the two-dimensional surface of a unit sphere. Following the usual procedure, we can parametrize the dynamical variables in terms of the polar angle θ and the azimuthal angle ϕ as $X = \sin\theta\cos\phi$, $Y = \sin\theta\sin\phi$, and $Z = \cos\theta$. In terms of these new (θ,ϕ) variables, the above map looks very complicated, and therefore we do not display that map. Moreover, during our numerical iterations we use the above three-dimensional form of the map, and after every iteration we get back the corresponding (θ,ϕ) from the relations $\cos\theta = Z$ and $\phi = \tan^{-1}(Y/X)$, where $\cos\theta$ and ϕ are the canonical coordinates on the sphere. In Fig. 1, we have presented the phase-space diagrams of the single top for different values of the parameter k. For $k = 1.0$ and $k = 2.0$, the phase space is mostly occupied by regular orbits. As we further increase the value of k, we can see the well-known kolmogrou-Arnold-moser scenario. Finally, at $k = 6.0$, the phase space is mostly covered by the chaotic sea, with very tiny islands. The dark circle, marking the point $(\theta,\phi) = (0.89, 0.63)$ in all the phase-space diagrams, is representing the point at which we will construct our initial wave packet. The quantities presented in all the figures are dimensionless.

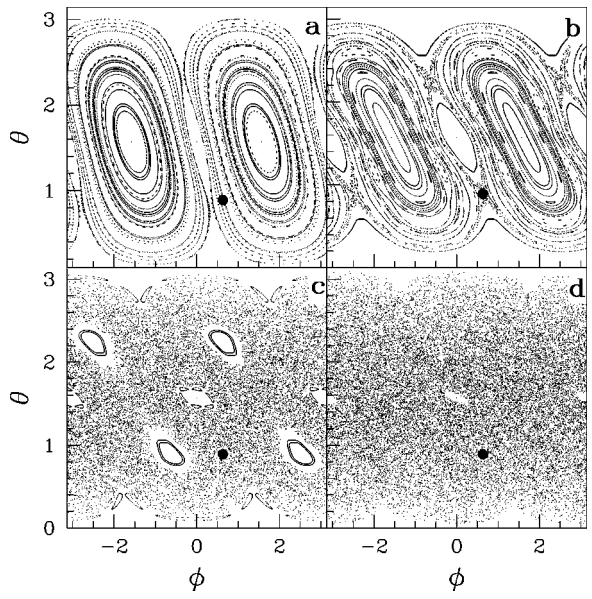

FIG. 1. Phase-space pictures of the single top, corresponding to different parameter values, are presented. (a) $k = 1.0$: The phase space is mostly regular. (b) $k = 2.0$: The phase space is still very much regular, but now a thin stochastic layer is visible at the separatrix. (c) $k = 3.0$: The phase space is truly mixed type. Regular elliptic islands are visible inside the chaotic region. (d) $k = 6.0$: The phase space is mostly covered by the chaotic region with few tiny elliptic islands. The solid circle is the point at which we will construct the initial wave packet.

C. Initial wave packet

We use a generalized SU(2) coherent state or the directed angular momentum state [28] as our initial state for the individual tops and this state is given in $|j,m_i\rangle$ basis as

$$\langle j,m_i|\theta_0,\phi_0\rangle = (1+|\gamma|^2)^{-j}\gamma^{j-m_i}\sqrt{\binom{2j}{j+m_i}}, \tag{12}$$

where $\gamma \equiv \exp(i\phi_0)\tan(\theta_0/2)$. For the coupled top, we take

the initial state as the tensor product of the directed angular momentum state corresponding to individual tops. Now on, we will write $|j,m_i\rangle$ as $|m_i\rangle$ for notational simplification. Explicitly in $|m_i\rangle$ basis this initial product state can be written as [13]

$$|\psi(0)\rangle = \sum_{m_1,m_2=-j}^{+j} \langle m_1,m_2|\psi(0)\rangle |m_1,m_2\rangle = \sum_{m_1,m_2=-j}^{+j} \langle m_1|\theta_0^1,\phi_0^1\rangle\langle m_2|\theta_0^2,\phi_0^2\rangle |m_1,m_2\rangle, \tag{13}$$

where $\langle m_i|\theta_0^i,\phi_0^i\rangle, i=1,2$, can be obtained from Eq. (12).

Now we have the evolution $|\psi(n)\rangle = U_T|\psi(n-1)\rangle = U_T^2|\psi(n-2)\rangle = \ldots = U_T^n|\psi(0)\rangle$. Even though, the numerical iteration scheme for the above evolutions have already been presented in Ref. [13], here we again present that for the sake of completeness. From Ref. [13], we have

$$\langle s_1,s_2|\psi(n)\rangle = \exp\left(-i\frac{\epsilon}{j}s_1s_2\right)\sum_{m_1,m_2=-j}^{+j}\langle s_1|U_1|m_1\rangle \times\langle s_2|U_2|m_2\rangle\langle m_1,m_2|\psi(n-1)\rangle, \tag{14}$$

where

$$\langle s_1|U_1|m_1\rangle = \exp\left(-i\frac{k}{2j}s_1^2\right)d^{(j)}_{s_1m_1}\left(\frac{\pi}{2}\right). \tag{15}$$

$d^{(j)}_{s_1m_1}(\pi/2)$ is the Wigner rotation matrix [30]:

$$d^{(j)}_{s_1m_1}\left(\frac{\pi}{2}\right) = \frac{(-1)^{s_1-m_1}}{2^j}\binom{2j}{j-s_1}^{1/2}\binom{2j}{j+m_1}^{-1/2} \times\sum_k (-1)^k\binom{j-s_1}{k}\binom{j+s_1}{k+s_1-m_1}. \tag{16}$$

The main problem in calculating the Wigner rotation matrix lies in the calculation of the above sum. Defining that sum as V_{m_1}, and starting from $V_{-j}=1$ and $V_{-j+1}=2s_1$, we can get the other V_{m_1} recursively by using the following relation [31]:

$$(j-m_1+1)V_{m_1-1}-2s_1V_{m_1}+(j+m_1+1)V_{m_1+1}=0.$$

Besides the Wigner rotation matrix can be expressed in terms of Jacobi polynomials and of different hypergeometric functions [32]. However, we have followed the above recursive scheme.

D. Measures of entanglement

All the previous studies on the connection between entanglement and chaos, were based on pure states of bipartite system, where the von Neumann entropy S_V and the Linear entropy S_R of the RDMs were natural measures of entanglement. The definition of these entropies are:

$$S_V(n) = -\mathrm{Tr}_1[\rho_1(n)\ln\rho_1(n)] = -\mathrm{Tr}_2[\rho_2(n)\ln\rho_2(n)] \tag{17}$$

and

$$S_R(n) = 1-\mathrm{Tr}_1[\rho_1^2(n)] = 1-\mathrm{Tr}_2[\rho_2^2(n)], \tag{18}$$

where ρ_1 and ρ_2 are the RDMs corresponding to the first and the second top, respectively. In the eigenbasis of the RDM,

$$S_V(n) = -\sum_i \lambda_i\ln\lambda_i, \tag{19}$$

$$S_R(n) = 1-\sum_i \lambda_i^2, \tag{20}$$

where λ_i's are the eigenvalues of the RDMs.

E. Reduced Husimi function

Since the phase space of the coupled tops is four dimensional ($S^2\times S^2$), it is not possible to visualize the wave packet dynamics on such a phase space. Therefore, we use an approximate numerical way to visualize the behavior of the time evolving state $|\psi(n)\rangle$ in any one of its subspaces. We call this method *reduced Husimi function* and it is defined in the following way. Consider a state $|\psi\rangle$ in the angular momentum basis $|m_1,m_2\rangle$, i.e.,

$$|\psi\rangle = \sum_{m_1,m_2} a_{m_1m_2}|m_1,m_2\rangle. \tag{21}$$

The Husimi function of $|\psi\rangle$ is $|\langle z_1;z_2|\psi\rangle|^2$, where

$$\langle z_1;z_2|\psi\rangle = \sum_{m_1,m_2} a_{m_1m_2}\langle z_1|m_1\rangle\langle z_2|m_2\rangle, \tag{22}$$

and $|z_i\rangle\equiv|\theta_i,\phi_i\rangle$ are the directed angular momentum states (atomic coherent states). We define reduced Husimi function corresponding to first subspace,

$$\rho_{1H}(z_1) = \int_{z_2}|\langle z_1;z_2|\psi\rangle|^2 d\mu(z_2), \tag{23}$$

where $d\mu(z_2)$ is the Haar measure

$$d\mu(z_2) = \frac{2j+1}{4\pi}\sin\theta_2\, d\theta_2\, d\phi_2. \tag{24}$$

Since the phase space of a kicked top is the surface of a sphere of unit radius, the total phase space area is 4π. Therefore for the kicked top whose Hilbert space dimension is $N=2j+1$, volume of the Planck cell is $4\pi/(2j+1)$. Hence the above mentioned Haar measure $d\mu(z)$ is equal to the number of Planck cells present in the infinitesimal area $dz=\sin\theta d\theta d\phi$. The integration of $d\mu(z)$ over whole phase space will give total number of Planck cells $N=2j+1$ present in the whole phase space. One can also write the above expression, Eq. (23), as

$$\rho_{1H}(\theta_1,\phi_1)=\langle\theta_1,\phi_1|\frac{2j+1}{4\pi}\Bigg[\int_{\theta_2}\int_{\phi_2}\langle\theta_2,\phi_2|\psi\rangle \times\langle\psi|\theta_2,\phi_2\rangle\sin\theta_2\,d\theta_2\,d\phi_2\Bigg]|\theta_1,\phi_1\rangle. \tag{25}$$

The above integral is just the partial trace of the density matrix $|\psi\rangle\langle\psi|$ over the second subspace, and hence it gives the RDM corresponding to the first subspace. Therefore,

$$\rho_{1H}(\theta_1,\phi_1)=\langle\theta_1,\phi_1|\rho_1|\theta_1,\phi_1\rangle, \tag{26}$$

where ρ_1 is the RDM of the first subspace. Therefore, the reduced Husimi function is just the Husimi function of the RDM. We can write $\rho_1=\Sigma_{i=1}^{N}\lambda_i|e_i\rangle\langle e_i|$, where λ_i's are the eigenvalues of ρ_1 and $|e_i\rangle$'s are the corresponding eigenstates. These $|e_i\rangle$'s are also called Schmidt vectors. Therefore,

$$\rho_{1H}(\theta_1,\phi_1)=\sum_{i=1}^{N}\lambda_i|\langle\theta_1,\phi_1|e_i\rangle|^2. \tag{27}$$

Thus, the reduced Husimi function can also be expressed as the weighted sum of the Husimi functions of the Schmidt vectors, where the weight factors are the eigenvalues of the RDM. Identically, we can define reduced Husimi function for the second subspace, and is given by

$$\rho_{2H}(\theta_2,\phi_2)=\sum_{i=1}^{N}\lambda_i|\langle\theta_2,\phi_2|d_i\rangle|^2, \tag{28}$$

where $|d_i\rangle$'s are the Schmidt vectors of the second subspace.

III. SECOND MOMENT OF HUSIMI FUNCTION: A MEASURE OF COMPLEXITY OF A QUANTUM STATE

Reduced Husimi function technique is useful for the visualization of the behavior of the time evolving state on the phase space. Moreover, we want a phase-space measure of the complexity of any state to relate it with the entanglement. There already exists a good measure of that complexity based on the Husimi distribution function, $\rho_H=\langle z|\rho|z\rangle$, called ''classical entropy'' or Wehrl entropy [33] and that is given by

$$S(\rho_H)=\int d\mu(z)\rho_H\ln\rho_H. \tag{29}$$

However, it is difficult to determine the above quantity due to the presence of the logarithmic function. Therefore, following a recent proposal [34], we consider inverse of the ''second moment of the Husimi function'' $W_2(\rho_H)$ as a measure complexity of quantum states. This measure is defined as

$$W_2(\rho_H)=\frac{1}{M_2(\rho_H)}, \tag{30}$$

where

$$M_2(\rho_H)=\int d\mu(z)\rho_H^2. \tag{31}$$

The quantity W_2 represents the effective phase space occupied by the Husimi function of the state ρ and its unit is Planck's cell volume. We note that a similar kind of quantity, based on the Wigner function, has been introduced and studied as a measure of the complexity of quantum states in phase space [35] many years ago.

We can now define a quantity $\Delta N_{\text{eff}}\equiv W_2(\rho_H)/N$ as the fraction of the total number of Planck cells ($N=2j+1$) occupied by the state ρ. Since the total number of Planck cells is equal to the Hilbert space dimension, we can define ΔN_{eff} also as the rough measure of the fraction of the Hilbert space occupied by the above state. The above definitions of ΔN_{eff} are valid for the single top. For the coupled tops, phase space is four dimensional. Here, we can define ΔN_{eff} for any one of its subspaces. However, the only difference between these two cases is that ρ is a pure state for the single top whereas for the coupled tops, ρ is a mixed state. Here we have studied the time evolution of ΔN_{eff} for the single top and also for the coupled tops.

A. Single top

In the single top case, we have again considered SU(2) coherent state $|\psi(0)\rangle=|\theta_0,\phi_0\rangle$, which we have already defined in Eq. (12), as the initial state. We have constructed this state at the point $(\theta_0,\phi_0)=(0.89,0.63)$, and evolved it with repeated applications of the single top evolution operator U. The time evolution operator U, defined between two consecutive kicks, is given as

$$U=\exp\left(-i\frac{\pi}{2}J_y\right)\exp\left(-i\frac{k}{2j}J_z^2\right). \tag{32}$$

For the single top case, ΔN_{eff} at time n is

$$\Delta N_{\text{eff}}=\frac{1}{(2j+1)M_2[|\psi(n)\rangle]},$$

where

$$M_2[|\psi(n)\rangle]=\int d\mu(z)|\langle z|\psi(n)\rangle|^4 \tag{33}$$

and $|\psi(n)\rangle=U^n|\psi(0)\rangle$. In Fig. 2, we have shown time evolution of ΔN_{eff} for different k values. For $k=1.0$, the initial state is inside the elliptic region, and therefore, time evolution of this state is governed by the elliptic orbits on which it is initially placed. Since the evolution of this state is in some sense trapped by the elliptic orbits, it has little or no access to many parts of the phase space. Consequently, the maximum value of ΔN_{eff} is very small. After reaching its maxima, there are many oscillations in the time evolution of ΔN_{eff} due to partial and full revival of the time evolving state $|\psi(n)\rangle$. This particular issue of quantum revival of the time evolving state in such mixed systems warrant a separate study. Now at

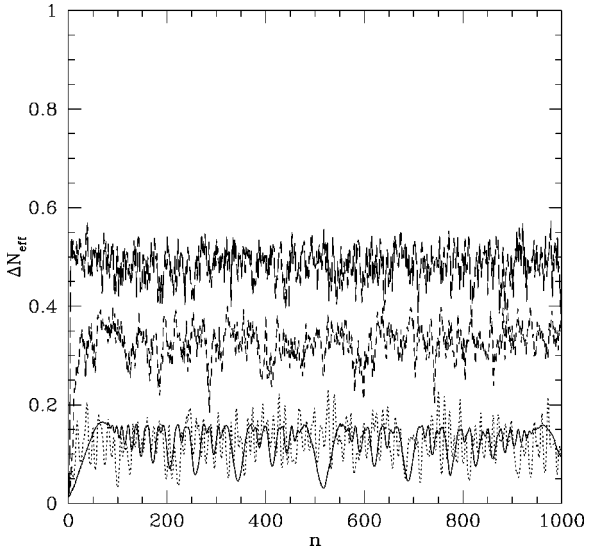

FIG. 2. Evolution of ΔN_{eff} is presented for the single top. For the nonchaotic cases ($k=1.0$ and $k=2.0$), denoted by solid and dotted line, respectively, maximum value of ΔN_{eff} is very less. That means, the time evolving state has very little access over the phase space. However, for chaotic cases ($k=3.0$ and $k=6.0$), maximum value of ΔN_{eff} is also not large. For the strongly chaotic case ($k=6.0$), the average value of the maxima is about 0.5.

$k=2.0$, the initial state is inside a stochastic layer present at the separatrix and consequently its dynamics is restricted by and large to be inside that stochastic layer. Naturally, for this case, the maxima of ΔN_{eff} is again small. For $k=3.0$, the phase space is of a truly mixed type, with a significant measure of chaotic orbits. In this case, the initial state is inside the chaotic region. Therefore, time evolution of this state is governed by the chaotic dynamics and this state has access over chaotic region of the phase space. Since the size of the chaotic region is large, hence the maxima of ΔN_{eff} is larger (~ 0.35). When $k=6.0$, the phase space is mostly covered by the chaotic region, with few visible tiny regular islands. The time evolving state has now almost full access over the phase space. However, we observed that ΔN_{eff} reaches maximum around 0.5 and then fluctuates around that value. That means, for this strong chaotic case, the time evolving *pure* state has access over only half of the phase space. This typical behavior of ΔN_{eff} for strongly chaotic case can be explained by RMT in the following way.

In the angular momentum basis $\{|m\rangle\}$,

$$M_2[|\psi(n)\rangle] = \sum_{i,k} \sum_{l,m} \langle i|\psi(n)\rangle\langle\psi(n)|k\rangle\langle l|\psi(n)\rangle \times \langle\psi(n)|m\rangle \int d\mu(z)\langle z|i\rangle\langle k|z\rangle\langle z|l\rangle\langle m|z\rangle. \tag{34}$$

After performing the above integral (see Appendix B),

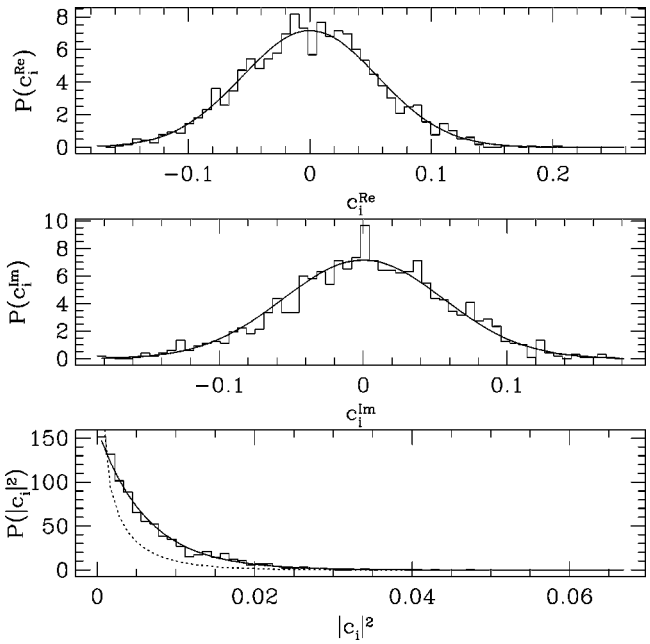

FIG. 3. Distribution of the components of the time evolving state, evolving under strongly chaotic single top dynamics is presented. Top and middle windows are showing that the real and the imaginary part of the components of the time evolving state are Gaussian distributed random numbers with *zero* mean and the variance is $1/\sqrt{N}$, where $N=2j+1$ is the Hilbert space dimension of the top. In this case $j=80$. Bottom window is showing that the distribution of the square of the absolute values of the components of the time evolving state are exponentially distributed. This is a typical property of the components of a GUE distributed vector. Dotted line represents the Gaussian orthogonal ensemble (GOE) distribution.

$$M_2[|\psi(n)\rangle] = \sum_{i,k} \sum_{l,m} \langle i|\psi(n)\rangle\langle\psi(n)|k\rangle\langle l|\psi(n)\rangle \times \langle\psi(n)|m\rangle F(2j;i,k,l,m)\,\delta_{i+l,k+m}, \tag{35}$$

where

$$F(2j;i,k,l,m) = \frac{2j+1}{(4j+1)!}\sqrt{\binom{2j}{j-i}\binom{2j}{j-k}\binom{2j}{j-l}\binom{2j}{j-m}} \times (2j-i-l)!(2j+i+l). \tag{36}$$

Let us assume, in the angular momentum basis,

$$|\psi(n)\rangle = \sum_m c_m|m\rangle. \tag{37}$$

In Fig. 3, we have presented the distribution of the real and the imaginary part of the coefficients c_m. They are indeed Gaussian distributed random numbers. Moreover, in this figure, we have also presented the distribution of $|c_m|^2$. This figure shows that $|c_m|^2$ are exponentially distributed, which is a typical property of the elements of a Gaussian unitary ensemble (GUE) distributed random vector. Therefore, we can assume that the distribution of $\{c_m\}$ are GUE type. For

GUE case, RMT average of a quantity identical to $M_2[|\psi(n)]$ has been calculated in a recent paper [36], and according to that,

$$\langle M_2[|\psi(n)]\rangle = \frac{2}{N+1}, \quad \text{where} \quad N=2j+1, \tag{38}$$

where the angular bracket $\langle\rangle$ represents RMT averaged value. Using the above expression, we have

$$\langle \Delta N_{\text{eff}}\rangle = \frac{N+1}{2N} = \frac{1}{2}\left(1+\frac{1}{N}\right) \tag{39}$$

and for large N limit,

$$\langle \Delta N_{\text{eff}}\rangle \simeq 0.5. \tag{40}$$

This is the saturation value of ΔN_{eff}, which was observed in strongly chaotic case $k=6.0$.

B. Coupled tops

In the preceding section, we have presented reduced Husimi function technique to visualize the behaviors of the time evolving state of the coupled tops on any one of its subspaces. However, to measure the complexity of this state in any one of its subspaces, we have to define ΔN_{eff} in a subspace. We have defined ΔN_{eff} for a given subspace as

$$\Delta N_{\text{eff}} = \frac{1}{(2j+1)M_2(\rho_{iH})}, \tag{41}$$

where

$$M_2(\rho_{iH}) = \int d\mu(z_i)\langle z_i|\rho_i|z_i\rangle, \tag{42}$$

and $i=1,2$ representing different subspaces. In Fig. 4, we have presented the time evolution of the above mentioned ΔN_{eff} for different dynamics (different k values) and for different coupling strengths ϵ. When coupling strength is very weak ($\epsilon=10^{-4}$), time evolution of ΔN_{eff} for different dynamics are practically identical to that which we have observed in the case of single tops. Therefore, for this coupling strength, effect of the dynamics of one top on the other top is very small and two tops are very close to two uncoupled systems. For other coupling strengths, the maxima of ΔN_{eff} has not changed much for the nonchaotic cases ($k=1.0$, and $k=2.0$). When $\epsilon=10^{-3}$, for the chaotic cases ($k=3.0$, and $k=6.0$), ΔN_{eff} first reaches the saturation value which is observed in the case of single tops and then it increases approximately linearly with time. However, for the stronger coupling ($\epsilon=10^{-2}$), it is not possible to divide the time evolution of ΔN_{eff}, for the chaotic cases, into two distinct time regimes. In these cases, ΔN_{eff} saturates at much higher values than the maxima of ΔN_{eff} observed in single top. For the strongly chaotic case $k=6.0$, ΔN_{eff} saturates at a value that is very slightly less than unity. This saturation of ΔN_{eff} can be also explained by RMT, which we now proceed to do.

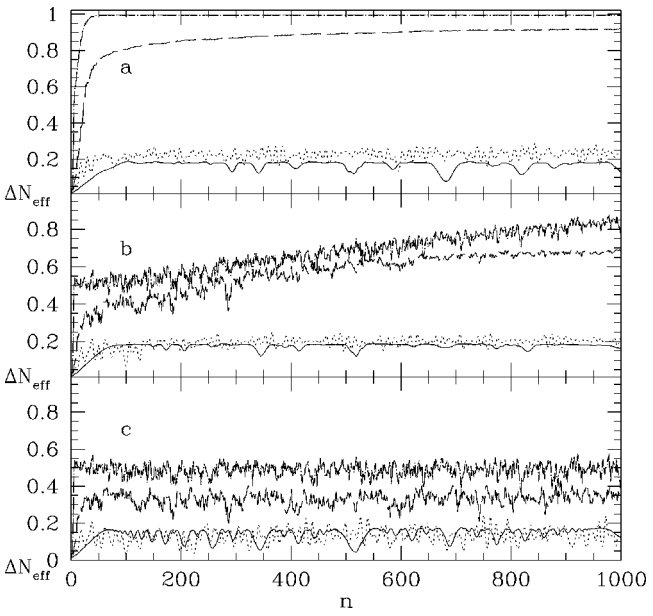

FIG. 4. Evolution of ΔN_{eff} corresponding to coupled kicked tops is presented. Solid lines and dotted lines are representing the results corresponding to nonchaotic cases ($k=1.0$ and $k=2.0$, respectively). Dashed lines are representing the mixed case ($k=3.0$) and dash-dot lines are showing the results corresponding to strongly chaotic case ($k=6.0$). The top window representing the results for the stronger coupling strength ($\epsilon=10^{-2}$), middle window is showing the results for the intermediate coupling strength ($\epsilon=10^{-3}$) and the bottom window is for the weak coupling case ($\epsilon=10^{-4}$).

In the angular momentum basis, second moment of the Husimi function of the reduced state, say for the first subsystem, at time n is

$$M_2(\rho_{1H}) = \sum_{i,k}\sum_{l,m}(\rho_1)_{ik}(\rho_1)_{lm}\int d\mu(z_1)\langle z_1|i\rangle\langle k|z_1\rangle\langle z_1|l\rangle \times\langle m|z_1\rangle. \tag{43}$$

After performing the above integral, we have

$$M_2(\rho_{1H}) = \sum_{i,k}\sum_{l,m}(\rho_1)_{ik}(\rho_1)_{lm}F(2j;i,k,l,m)\,\delta_{i+l,k+m} \tag{44}$$

where $F(2j;i,k,l,m)$ has already been given in Eq. (36). If we write down the above expression in the eigenbasis of the RDM ρ_1, then we have

$$\begin{aligned} M_2(\rho_{1H}) &= \sum_{\alpha,\beta=1}^{N}\lambda_\alpha\lambda_\beta\sum_{i,k}\sum_{l,m}\langle i|\phi_\alpha\rangle\langle\phi_\alpha|k\rangle\langle l|\phi_\beta\rangle \\ &\quad\times\langle\phi_\beta|m\rangle F(2j;i,k,l,m)\,\delta_{i+l,k+m} \\ &= \sum_{\alpha}\lambda_\alpha^2\sum_{i,k}\sum_{l,m}\langle i|\phi_\alpha\rangle\langle\phi_\alpha|k\rangle\langle l|\phi_\alpha\rangle \\ &\quad\times\langle\phi_\alpha|m\rangle F(2j;i,k,l,m)\,\delta_{i+l,k+m} \end{aligned} \tag{45}$$

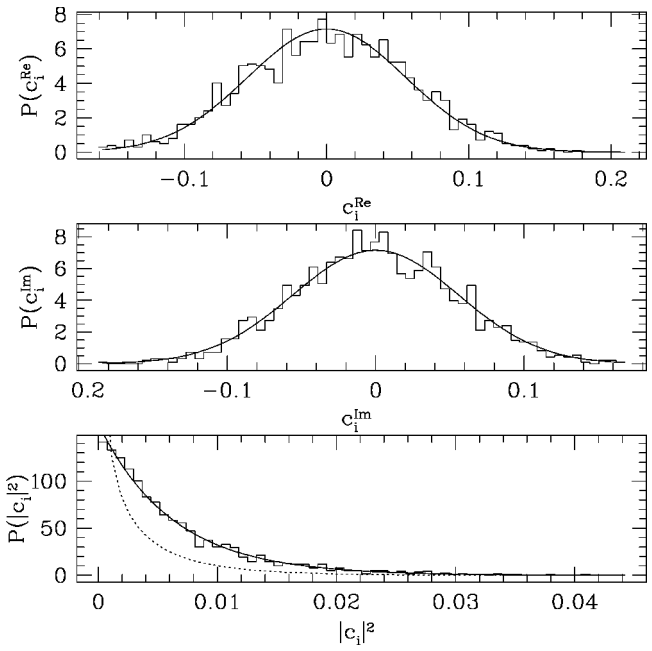

FIG. 5. Distribution of the components of the eigenvectors of the RDM, corresponding to which entanglement production has reached the statistical bound. The top and the middle window shows that the real and the imaginary part of the components of these eigenvectors of RDM are Gaussian distributed random numbers with *zero* mean and the variance is $1/\sqrt{N}$. Here $N=2j+1=161$. The bottom window is showing that the distribution of the absolute square of the eigenvectors of the RDM are exponentially distributed. Therefore, the eigenvectors of the RDM are GUE distributed. Dotted line represents the GOE distribution.

$$+\sum_{\substack{\alpha,\beta\\ \alpha\neq\beta}}\lambda_\alpha\lambda_\beta\sum_{i,k}\sum_{l,m}\langle i|\phi_\alpha\rangle\langle\phi_\alpha|k\rangle\langle l|\phi_\beta\rangle \times\langle\phi_\beta|m\rangle F(2j;i,k,l,m)\,\delta_{i+l,k+m}$$

$$\equiv\sum_\alpha\lambda_\alpha^2 Q_{\alpha\alpha}^2+\sum_{\substack{\alpha,\beta\\ \alpha\neq\beta}}\lambda_\alpha\lambda_\beta Q_{\alpha\beta}^2$$

$$\text{where}\quad Q_{\alpha\alpha}^2=\sum_{i,k}\sum_{l,m}\langle i|\phi_\alpha\rangle\langle\phi_\alpha|k\rangle\langle l|\phi_\alpha\rangle \times\langle\phi_\alpha|m\rangle F(2j;i,k,l,m), \tag{46}$$

$$\text{and}\quad Q_{\alpha\beta}^2=\sum_{i,k}\sum_{l,m}\langle i|\phi_\alpha\rangle\langle\phi_\alpha|k\rangle\langle l|\phi_\beta\rangle \times\langle\phi_\beta|m\rangle F(2j;i,k,l,m), \tag{47}$$

where $\{\lambda_\alpha,|\phi_\alpha\rangle\}$ are the eigenvalues and the eigenvectors of the RDM ρ_1.

In Fig. 5, we have presented the distribution of the real and the imaginary part of the components of the eigenvectors $\{|\phi_\alpha\rangle\}$ of the RDM ρ_1. This figure shows that the real and the imaginary part of $\{|\phi_\alpha\rangle\}$ are Gaussian distributed random numbers. Moreover, Fig. 5 also shows that the distribution of the absolute square of the components of $\{|\phi_\alpha\rangle\}$ is GUE type. Therefore, from the recent calculation [36], we can again use RMT average values of $Q_{\alpha\alpha}^2$ and $Q_{\alpha\beta}^2$ to get RMT average value of $M_2(\rho_{1H})$ as,

$$\langle M_2(\rho_{1H})\rangle=\frac{2}{N+1}\left\langle\sum_\alpha\lambda_\alpha^2\right\rangle+\frac{1}{N+1}\left\langle\sum_{\substack{\alpha,\beta\\ \alpha\neq\beta}}\lambda_\alpha\lambda_\beta\right\rangle$$
$$=\frac{2}{N+1}\left\langle\sum_\alpha\lambda_\alpha^2\right\rangle+\frac{1}{N+1}\left[1-\left\langle\sum_\alpha\lambda_\alpha^2\right\rangle\right]$$
$$=\frac{1}{N+1}\left(1+\left\langle\sum_\alpha\lambda_\alpha^2\right\rangle\right). \tag{48}$$

We know from our earlier work [15],

$$\left\langle\sum_\alpha\lambda_\alpha^2\right\rangle=\frac{2N+1}{N^2+2}. \tag{49}$$

Therefore, we have,

$$\langle M_2(\rho_{1H})\rangle=\frac{1}{N+1}\left(1+\frac{2N+1}{N^2+2}\right). \tag{50}$$

Hence,

$$\langle\Delta N_{\text{eff}}\rangle=\frac{1}{N\langle M_2(\rho_{1H})\rangle}=\frac{(N+1)(N^2+2)}{N(N^2+2N+3)}. \tag{51}$$

In the large N limit,

$$\langle\Delta N_{\text{eff}}\rangle=\frac{N+1}{N+2}+O\left(\frac{1}{N^2}\right)\lesssim 1.0. \tag{52}$$

This is the saturation value of ΔN_{eff}, which we have observed in the strongly chaotic ($k=6.0$) and strongly coupled ($\epsilon=10^{-2}$) case. We emphasize that this is nearly twice that of pure states in a single top. Thus roughly speaking the effect of strongly coupling to another chaotic system doubles the phase space access of a state.

IV. NUMERICAL RESULTS

A. Classical phase space

In Fig. 1, we have presented the phase-space picture of the single kicked top for different parameter values. For $k=1.0$, as shown in Fig. 1(a), the phase space is mostly covered by regular orbits, without any visible stochastic region. Our initial wave packet, marked by a solid circle at the coordinate (0.89,0.63), is on the regular elliptic orbits. As we further increase the parameter, regular region becomes smaller. Figure 1(b) is showing the phase space for $k=2.0$. Still the phase space is mostly covered by the regular region, but now we can observe a thin stochastic layer at the separatrix. In this case, the initial wave packet is on the separatrix. For the change in the parameter value from $k=2.0$ to $k=3.0$, there is significant change in the phase space. At $k=3.0$, shown in Figure 1(c), the phase space is of a truly mixed type. The size of the chaotic region is now very large

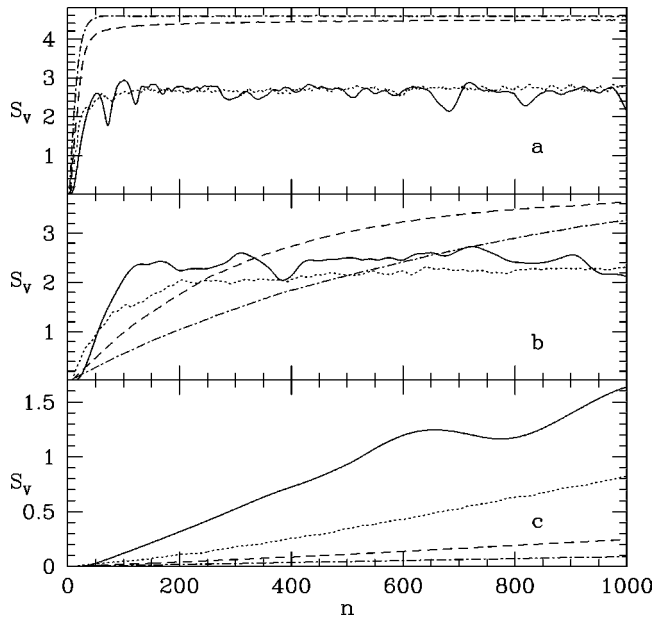

FIG. 6. Time evolution of the von Neumann entropy in coupled kicked tops is presented for different coupling strengths and for different underlying classical dynamics. (a) $\epsilon=10^{-2}$. (b) $\epsilon=10^{-3}$. (c) $\epsilon=10^{-4}$. Solid line represents $k=1.0$, dotted line corresponds to $k=2.0$, dashed line is for $k=3.0$, and dash-dot line represents $k=6.0$.

with few regular islands. At this parameter value, the initial wavepacket is inside the chaotic region. Fig. 1(d) is showing the phase space for $k=6.0$. Now the phase space is mostly covered by the chaotic region, with very tiny regular islands. Naturally, our initial wave packet is in the chaotic region.

B. Time evolution of the quantum entanglement

In Fig. 6, we have presented our results for the entanglement production in coupled kicked tops for the spin $j=80$. As we go from top to bottom window, coupling strength is decreasing by a factor of ten. Top window corresponds to $\epsilon=10^{-2}$, middle one is showing the results for $\epsilon=10^{-3}$, and the bottom window corresponds to the case $\epsilon=10^{-4}$. For each coupling strength, we have studied entanglement production for four different single top parameter values, whose corresponding classical phase-space picture has already been shown in Fig. 1.

1. Coupling $\epsilon=10^{-2}$

Let us first discuss the case of stronger coupling $\epsilon=10^{-2}$, whose results are presented in Fig. 6(a). It shows that there exists a saturation of S_V for $k=1.0$ and $k=2.0$, which are much smaller than the saturation value corresponding to highly chaotic cases such as when $k=6.0$. The saturation value of S_V for $k=6.0$ is the statistical bound $S_V=\ln(N)-\frac{1}{2}\simeq 4.57$ (where $N=161$), which can be understood from random matrix theory [15]. However for $k=3.0$, corresponding to a mixed classical phase space, S_V is still less than the above mentioned saturation value, indicating the influence of the regular regions.

These two distinct behaviors of the entanglement saturation can be understood from the underlying classical dynamics. For $k=1.0$, the initial unentangled state is the product of the coherent wave packet placed inside the elliptic region [see Fig. 1(a)] of each top. This initially unentangled state will become more and more entangled under the repeated application of the coupled top unitary operator U_T. Moreover, if one observes the evolution of the reduced Husimi function corresponding to each top, then it can be seen that the initially localized wave packet starts moving along the classical elliptic orbits on which it was initially placed and simultaneously it also spreads along those orbits.

However, one can observe some initial oscillations in the entanglement production, which is due to the fact that the entanglement production is mostly determined by the spreading of the wave packet along θ direction. As we know $\cos\theta_i=\lim_{j\to\infty}(J_{z_i}/j)$, therefore the spreading of the wave packet along θ direction determines how many eigenstates of J_{z_i}, which are also our basis states, are participating to construct the wave packet. Larger amount of spreading of the wave packet along the θ direction causes greater number of basis states to participate in the wave packet. Moreover, coupling between two tops is via interaction between J_{z_1} and J_{z_2}. Therefore, this interaction term will couple greater number of basis states and consequently leads to higher entanglement.

Initially, the spreading of the wave packet sometimes may become parallel to the ϕ direction and therefore its spreading along θ direction become less. Consequently, one can observe a dip in the entanglement production. Finally, the wave packet spreads all over the elliptic orbits and the entanglement production reaches its saturating maxima. In Fig. 7(a), we have shown the reduced Husimi function of the wave packet corresponding to the maxima (saturation) of the entanglement production. After reaching its saturation, there are again many dips in the entanglement production. These dips are also due to the small spreading of the wave packet along θ direction. However, the localization of the wave packet along θ direction are now happening due to fractional or full revival of the wave packet. These revivals are actually the single top behaviors which persists even under the interaction with other top. The quantum revivals of the wave packet are interesting phenomena of any quantum system and therefore it requires separate study, especially in this rather more complex setting.

At $k=2.0$, the center of the initial coherent state was inside the separatrix. Therefore, in its time evolution, the spreading of the wave packet was restricted to be inside the separatrix region. Finally, the wave packet spread over the separatrix region, and the entanglement production arrived at its saturation. The corresponding reduced Husimi function has been shown in Fig. 7(b). Moreover, the reduced Husimi function shows that even though the wave packet has spread over the whole separatrix region, its spread is not uniform. The wave packet is strongly localized at the unstable period-4 orbit. This strong localization of the wave packet is also a single top behavior which may also warrant separate study.

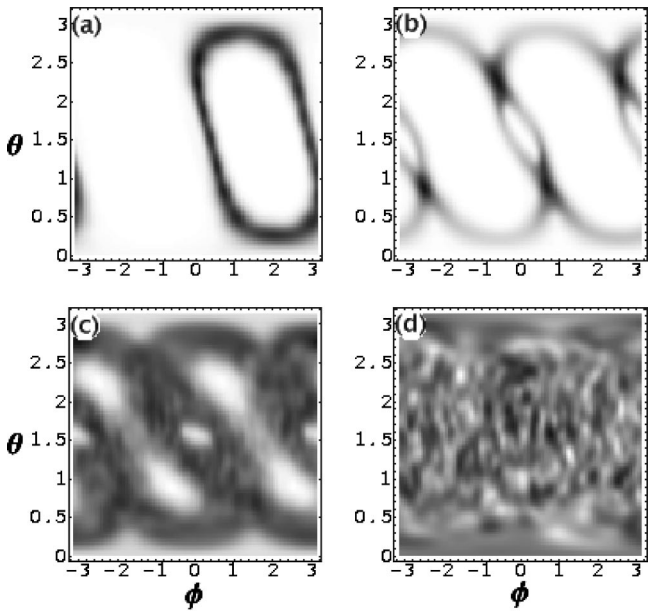

FIG. 7. Reduced Husimi functions of the time evolving state, evolving under U_T, are presented corresponding to the time at which the entanglement production is saturated. (a) $k=1.0$: The wave packet is spread over the elliptic orbits. (b) $k=2.0$: The wave packet is spread over the separatrix. It is also showing strong localization at the unstable period-4 orbit. (c) $k=3.0$: The wave packet is spread over the whole chaotic region. (d) $k=6.0$: At this parameter value, the phase space is mostly covered by the chaotic region, see Fig. 1. Consequently, the wave packet is spread over almost whole phase space.

At $k=3.0$ and $k=6.0$, the initial wave packets were inside the chaotic region. However, the saturation of the entanglement production are different for these two cases. This can be understood as the phase space of the kicked top is more mixed type for $k=3.0$ than the case $k=6.0$. Therefore, the size of the chaotic region is less for $k=3.0$ than its size corresponding to $k=6.0$. Consequently, the wave packet can spread over less of the phase space for $k=3.0$ than $k=6.0$. In Fig. 7(c), we have shown the spreading of the wave packet corresponding to this case. At $k=6.0$, since the phase space is almost fully chaotic, the wave packet can spread over almost whole phase space. In Fig. 7(d), we have shown reduced Husimi function corresponding to this strongly chaotic case.

As we know, there exists a universal bound on the entanglement for chaotic cases and that bound is given by, for the von Neumann entropy, $(S_V)_{\text{sat}}=\ln \gamma N$ where $\gamma=1/\sqrt{e}\simeq 0.6$. Now a natural question is whether there exists any such bound on entanglement of the form $\ln \gamma N'$, for the non-chaotic cases such as $k=1.0$ and $k=2.0$. If there exists really such an entanglement bound, then what is the N' in terms of N? We conjecture that N' is actually the effective dimension of the Hilbert space corresponding to those parameter values, i.e., $N'=N_{\text{eff}}=\Delta N_{\text{eff}} N$. Since we know the evolution of S_V and of ΔN_{eff}, we can determine the time evolution of that factor γ from the relation

$$\gamma=\frac{\exp(S_V)}{N'}=\frac{1}{N}\left[\frac{\exp(S_V)}{\Delta N_{\text{eff}}}\right]. \tag{53}$$

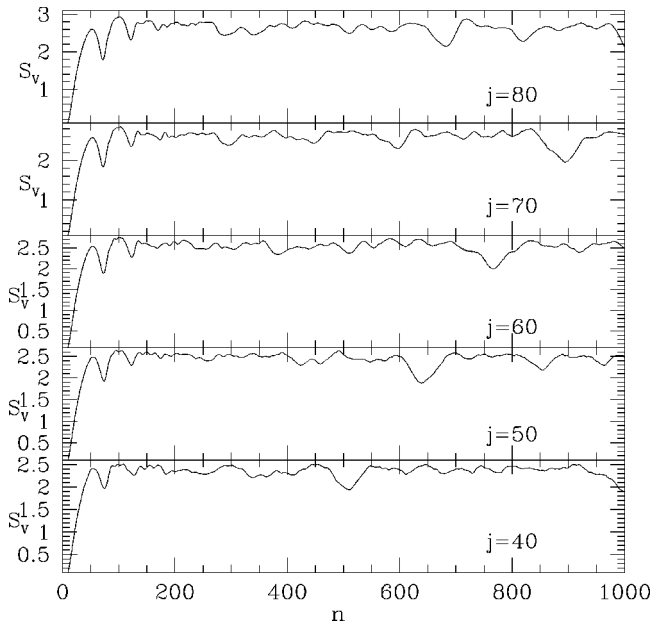

FIG. 8. Evolution of the von Neumann entropy, corresponding to the parameter value $k=1.0$, are presented for different Hilbert space dimensions ($N=2j+1$).

In Figs. 8 and 9, we have shown the evolution of S_V and ΔN_{eff} corresponding to $k=1.0$ for different Hilbert space dimensions. Using the above relation, we determine the evolution of γ for this k value and that is presented in Fig. 10. Initially there were some oscillations, later it fluctuates approximately around $\gamma\simeq 0.52-0.54$ for different Hilbert space dimensions. The solid line is showing the average value of γ at the saturation region. Figs. 11 and 12 are similarly showing the evolution of S_V and of ΔN_{eff} at $k=2.0$ corresponding to different Hilbert space dimensions. In Fig.

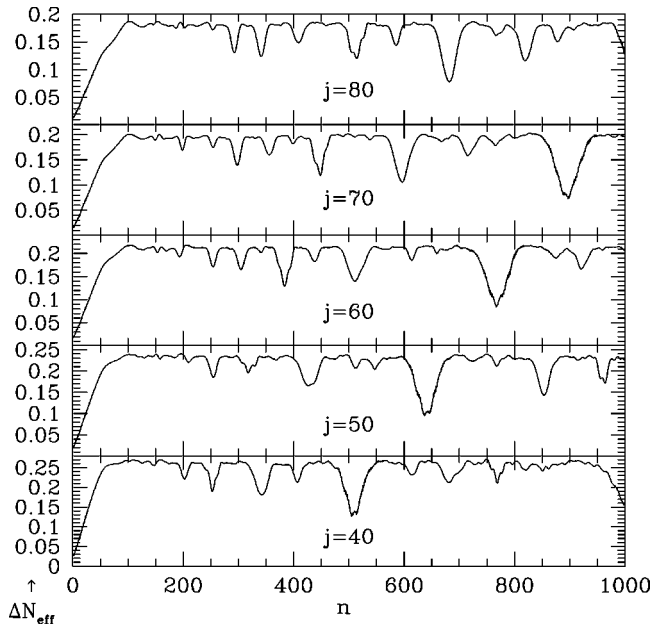

FIG. 9. Evolution of ΔN_{eff}, corresponding to $k=1.0$, are presented for different Hilbert space dimensions.

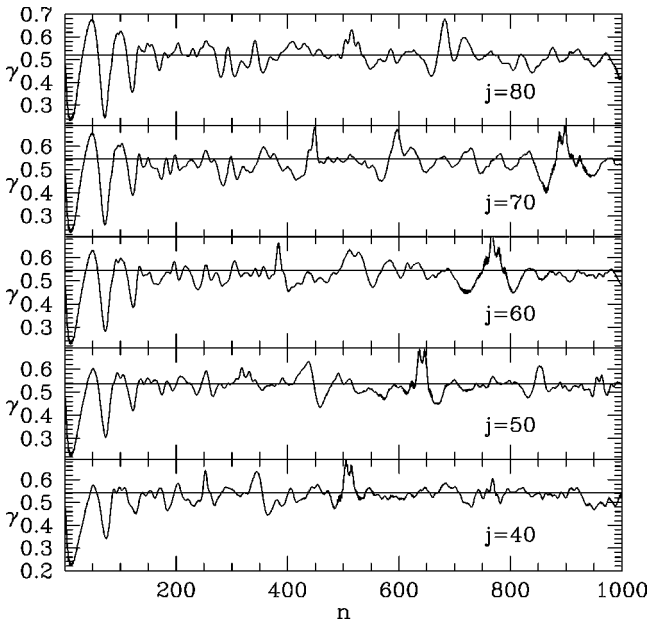

FIG. 10. Evolution of the factor γ are presented for different Hilbert space dimensions. This factor has been calculated numerically using Eq. (53). Here $k=1.0$.

13, we have shown the evolution of γ for this case. This figure is showing that at the saturation $\gamma \simeq 0.40-0.43$ for different Hilbert space dimensions. At the saturation, the factor γ is different for $k=1.0$ and $k=2.0$. This is essentially due to the fact that at $k=1.0$ and $k=2.0$, two different kind of dynamics are responsible for the spreading of the wave packet on phase space. At $k=1.0$, the wave packet has spread over the regular elliptic orbits, whereas at $k=2.0$ the wave packet has spread over a thin stochastic layer present at

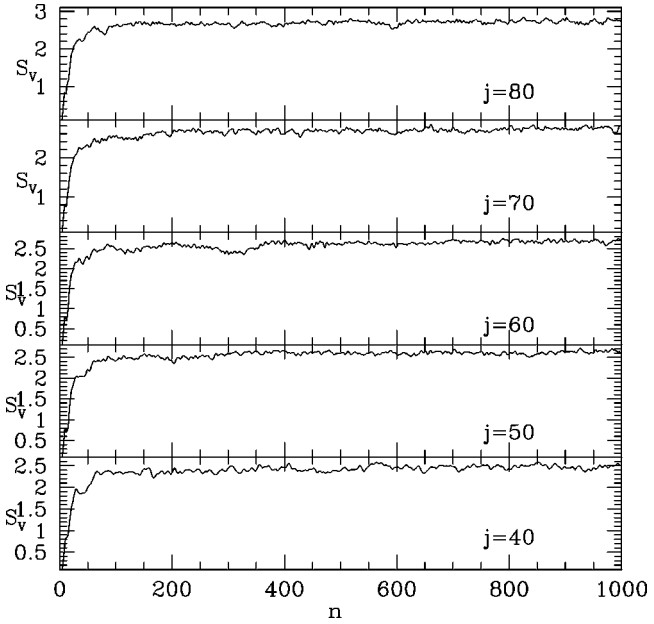

FIG. 11. Evolution of the von Neumann entropy, corresponding to the parameter value $k=2.0$, are presented for different Hilbert space dimensions.

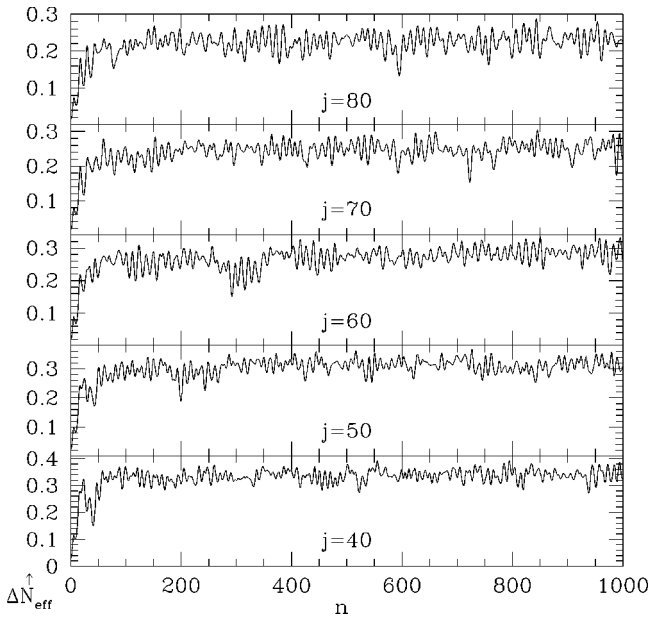

FIG. 12. Evolution of ΔN_{eff}, corresponding to $k=2.0$, are presented for different Hilbert space dimensions.

the separatrix. Even though we may not expect any universality in the case of integrable or near-integrable cases, we have found that for a given coupling strength and for a given classical dynamical behavior, the factor γ is more or less the same for different Hilbert space dimensions.

2. Coupling $\epsilon=10^{-3}$

Entanglement production corresponding to this coupling strength has been presented in Fig. 7(b). For the nonchaotic cases ($k=1.0$ and $k=2.0$), the saturation value of the en-

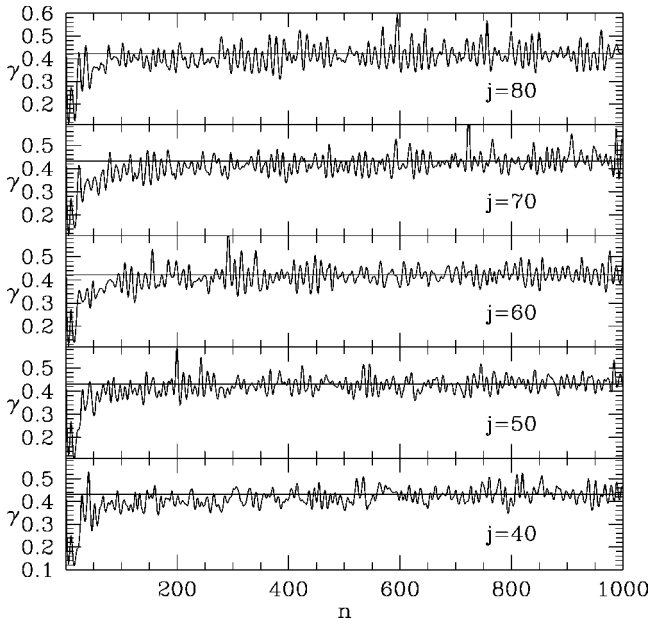

FIG. 13. Evolution of the factor γ are presented for different Hilbert space dimensions. This factor has been calculated numerically using Eq. (53). Here $k=2.0$.

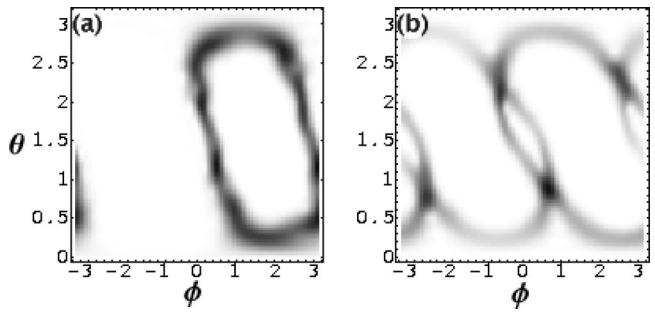

FIG. 14. Reduced Husimi functions of the time evolving wave packet are presented corresponding to the time $n=384$ at which the entanglement production gets saturated. (a) $k=1.0$. The wave packet is spread over the elliptic orbits, but the spreading is not uniform. (b) $k=2.0$. The wave packet is spread over the separatrix and shows strong localization on the unstable period-4 orbit. Here $\epsilon=10^{-3}$.

tanglement production is less than the entanglement saturation observed in the stronger coupling case ($\epsilon=10^{-2}$). For weaker coupling, the influence of one subsystem on the other subsystem becomes less, and the individual subsystems behave more like isolated quantum systems. Consequently, pure quantum effects play dominant role in the evolution of the wave packet. In Fig. 14, we have shown reduced Husimi function for $k=1.0$ and $k=2.0$ at the time $n=384$ when the entanglement production saturated. For $k=1.0$, the reduced Husimi function is showing that the wave packet has spread over the elliptic orbits, but not uniformly.

Now for $k=2.0$, at the entanglement saturation, the wave packet has spread as usual over the whole separatrix region. Moreover, it also shows localization at the same unstable period-4 orbit. However, the difference is that the wave packet is now more localized at a particular periodic point of that period-4 orbit which was very close to the initial wave packet. As we have seen in Fig. 4(b), within our observational time ($n=1000$), ΔN_{eff} has not reached any saturation value for the mixed and as well as for the chaotic cases. Moreover, for the strong chaos case, $k=6.0$, the ΔN_{eff} was well short of unity even after the observational time and consequently the wave packet has not got access over whole Hilbert space within this time of observation. Therefore, the entanglement production is well short of the known statistical bound $\ln(N)-\frac{1}{2}$.

3. Coupling $\epsilon=10^{-4}$

The entanglement production for this very weak coupling regime has been presented in Fig. 7(c). The entanglement production for this weak coupling has recently been explained by perturbation theory [16]. However, the formula for the entanglement production presented in that work is not valid for arbitrarily long times. In the following section we have presented an approximate formula for the entanglement production in coupled strongly chaotic systems. This formula explains the entanglement production for the case $k=6.0$. Here we have also observed that entanglement production is much larger for the nonchaotic cases than the chaotic cases. Rather, we can say that, for weakly coupled cases, the presence of chaos actually suppresses entanglement production.

V. ENTANGLEMENT PRODUCTION IN COUPLED STRONGLY CHAOTIC SYSTEM

Due to the relatively simple form of S_R, the linear entropy, it is easier to derive an approximate formula for its time evolution. Here we present an analytical formalism for the time evolution of S_R in coupled strongly chaotic systems.

Let us assume, the initial state is a product state, given as $|\psi(0)\rangle=|\phi_1(0)\rangle\otimes|\phi_2(0)\rangle$, where $|\phi_i(0)\rangle$'s are the states corresponding to individual subsystems. In general, the time evolution operator of a coupled system is of the form $U\equiv U_\epsilon U_0=U_\epsilon(U_1\otimes U_2)$, where U_ϵ is the coupling time evolution operator and U_i's are the time evolution operators of the individual subsystems. Furthermore, we have assumed

$$U_\epsilon=\exp(-i\epsilon H_{12}), \tag{54}$$

where $H_{12}=h^{(1)}\otimes h^{(2)}$, and $h^{(i)}$ are Hermitian local operators. For simplicity, we derive our formalism in the eigenbasis of $h^{(i)}$'s, i.e., $h^{(i)}|e_\alpha^{(i)}\rangle=e_\alpha|e_\alpha^{(i)}\rangle$, where $\{e_\alpha^{(i)},|e_\alpha^{(i)}\rangle\}$ are the eigenvalues and the corresponding eigenvectors of $h^{(i)}$.

The one step operation of U on $|\psi(0)\rangle$ will give

$$\langle e_\alpha^{(1)},e_\beta^{(2)}|\psi(1)\rangle=\exp(-i\epsilon e_\alpha^{(1)}e_\beta^{(2)})\langle e_\alpha^{(1)}e_\beta^{(2)}|\psi_0(1)\rangle, \tag{55}$$

where $|\psi(1)\rangle$ is the time evolving state of the full coupled system at time $n=1$ and $|\psi_0(1)\rangle$ is the same for the uncoupled system. From the above expression, one can get the RDM corresponding to one subsystem by tracing over the other subsystem. The RDM corresponding to the first subsystem is given by

$$\begin{aligned}[\rho_1(1)]_{\alpha\beta}&=\langle e_\alpha^{(1)}|\rho_1(1)|e_\beta^{(1)}\rangle\\&=\sum_\gamma\langle e_\alpha^{(1)},e_\gamma^{(2)}|\psi(1)\rangle\langle\psi(1)|e_\beta^{(1)},e_\gamma^{(2)}\rangle\\&=\sum_\gamma\exp[-i\epsilon(e_\alpha^{(1)}-e_\beta^{(1)})e_\gamma^{(2)}]\langle e_\alpha^{(1)},e_\gamma^{(2)}|\psi_0(1)\rangle\\&\quad\times\langle\psi_0(1)|e_\beta^{(1)},e_\gamma^{(2)}\rangle.\end{aligned} \tag{56}$$

Here we now assume that $|\psi_0(1)\rangle$ is a random vector. Consequently we can further assume that the components of $|\psi_0(1)\rangle$ are uncorrelated to the exponential term coming due to the coupling. Hence we have

$$\begin{aligned}[\rho_1(1)]_{\alpha\beta}&\simeq\frac{1}{N}\sum_\gamma\langle e_\alpha^{(1)},e_\gamma^{(2)}|\psi_0(1)\rangle\langle\psi_0(1)|e_\beta^{(1)},e_\gamma^{(2)}\rangle\\&\quad\times\sum_\delta\exp[-i\epsilon(e_\alpha^{(1)}-e_\beta^{(1)})e_\gamma^{(2)}]\\&=\frac{1}{N}[\rho_{10}(1)]_{\alpha\beta}\sum_\gamma\exp[-i\epsilon(e_\alpha^{(1)}-e_\beta^{(1)})e_\gamma^{(2)}],\end{aligned} \tag{57}$$

where N is the Hilbert space dimension of the first subsystem and ρ_{10} is the density matrix corresponding to the uncoupled top. If we proceed one more time step, then at the time $n=2$ we have

$$[\rho_1(2)]_{\alpha\beta} \simeq \frac{1}{N}|p(\epsilon)|^2 [\rho_{10}(2)]_{\alpha\beta} \sum_{\gamma} \exp[-i\epsilon(e_\alpha^{(1)} - e_\beta^{(1)})]$$

where

$$p(\epsilon) = \frac{1}{N^2} \sum_{\alpha,\beta} \exp(-i\epsilon e_\alpha^{(1)} e_\beta^{(2)}). \tag{58}$$

If we use the above assumptions upto any arbitrary time n, we obtain

$$[\rho_1(n)]_{\alpha\beta} = \frac{1}{N}|p(\epsilon)|^{2(n-1)} [\rho_{10}(n)]_{\alpha\beta} \times \sum_{\gamma} \exp[-i\epsilon(e_\alpha^{(1)} - e_\beta^{(1)}) e_\gamma^{(2)}]. \tag{59}$$

From the above expression, it is straightforward to calculate linear entropy and that is given as,

$$S_R(n) \simeq 1 - \frac{1}{N^4}|p(\epsilon)|^{4(n-1)} \times \sum_{\alpha,\beta} \sum_{\gamma,\delta} \exp[-i\epsilon(e_\alpha^{(1)} - e_\beta^{(1)})(e_\gamma^{(2)} - e_\delta^{(2)})]. \tag{60}$$

This is a general result, applicable to any coupled strongly chaotic systems of the form $U_\epsilon(U_1 \otimes U_2)$. Moreover, this result is valid for long time.

For the coupled kicked tops $H_{12} = J_{z_1} \otimes J_{z_2}/j$. Therefore, for this particular system, the above formula would become

$$S_R(n) \simeq 1 - \frac{1}{N^4} p(\epsilon)^{4(n-1)} \times \sum_{m_1, n_1 = -j}^{+j} \sum_{m_2, n_2 = -j}^{+j} \exp\left[-i\frac{\epsilon}{j}(m_1 - n_1)(m_2 - n_2)\right],$$

where

$$p(\epsilon) = \frac{1}{N^2} \sum_{m_1, m_2 = -j}^{+j} \exp\left(-i\frac{\epsilon}{j} m_1 m_2\right) \quad \text{and} \quad N = 2j+1. \tag{61}$$

In large j limit, we can substitute above sums by approximate integrals and then performing those integrals we get (for details, see Appendix C),

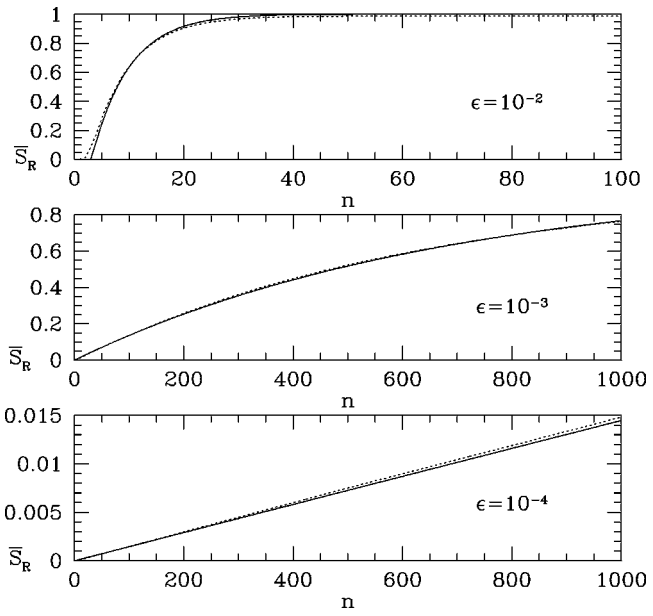

FIG. 15. Evolution of the linear entropy for the coupled strongly chaotic system is presented. The dotted line is the numerical results of the coupled kicked tops system. We choose $k=6.0$ for the first top and $k=6.1$ for the second top. The solid line is the theoretical estimation, given by Eq. (62).

$$S_R(n) \simeq 1 - p(\epsilon)^{4(n-1)} \left[\frac{2}{N}\left\{1 + \frac{\mathrm{Si}(2N\epsilon)}{\epsilon}\right\} - \left(\frac{1}{N\epsilon}\right)^2 \times \{1 - \cos(2N\epsilon) + \mathrm{Ci}(2N\epsilon) - \ln(2N\epsilon) - \gamma\}\right]$$

where

$$p(\epsilon) \simeq \frac{2}{N}\left[1 + \frac{1}{\epsilon}\mathrm{Si}\left(\frac{N\epsilon}{2}\right)\right]. \tag{62}$$

The functions Si and Ci are the standard *sine-integral* and *cosine-integral* function, respectively, while $\gamma = 0.577\,216\ldots$ is the Euler constant. In the above derivation we have not assumed, unlike the perturbation theory [16], any particular order of magnitude of the coupling strength ϵ. Therefore, as we demonstrate below, the above formula is applicable for nonperturbative coupling strengths as well.

In Fig. 15, we have shown the numerical result of the linear entropy (S_R) production in the coupled tops where the individual tops are strongly chaotic. Here we have considered many initial coherent states at different parts of the phase space and presented the linear entropy production, averaged over all these initial states, with time. In all our previous calculations we only considered the entanglement production on coupling identical tops, therefore, permutation symmetry was present. As in the above derivation, we have not assumed any special symmetry property, we break permutation symmetry by taking slightly nonidentical tops with $k=6.0$ for the first top and $k=6.1$ for the second top.

Figure 15 demonstrates that our theoretical estimation, denoted by the solid curve, is not only valid for weak coupling

case such as $\epsilon=10^{-4}$ but it also valid for sufficiently strong coupling cases such as $\epsilon=10^{-2}$. Moreover, this formula is applicable for very long times. If we consider weak coupling approximation, i.e., $j\epsilon\ll 1$, then the above formula will become approximately

$$S_R(n)\simeq\frac{2\epsilon^2j^2}{9}(n-1)+O(\epsilon^3j^3). \tag{63}$$

Therefore, at this weak coupling approximation, the entanglement production rate is $2\epsilon^2j^2/9$, which has been calculated in a recent publication [16] by very different means.

VI. SUMMARY

In this paper, our major goal was to study entanglement production in coupled kicked tops. Single kicked top is a well studied model of both classical and quantum chaotic system. The classical map corresponding to coupled kicked tops was presented in a previous publication, but was unfortunately incorrect. Hence, we have presented the correct classical map corresponding to the coupled kicked tops which is canonical. In the quantum case, we have studied the reduced Husimi function to visualize the behavior of the wave packet of a coupled system in any one of its subspaces. We have also studied a phase-space based measure of complexity of the time evolving state (denoted by $\Delta N_{\rm eff}$), which quantify the fraction of the total number of the Planck cells occupied by the Husimi function of a given state. As we have already mentioned that, for kicked top, this quantity is also approximately equal to the fraction of the Hilbert space occupied by a given state. We have studied this quantity for both single and coupled tops. It has been observed that, for the single top, the time evolving state can occupy maximum, in average, *half* of the total number of the Planck cell, i.e., $\Delta N_{\rm eff}=0.5$, and this happened for the strongly chaotic cases.

For nonchaotic and mixed cases, the time evolving state occupies even less number of Planck cells and it is reflected in smaller values of $\Delta N_{\rm eff}$. Following a recent result, using RMT, we have explained the fact that $\Delta N_{\rm eff}=0.5$ for the time evolving state corresponding to strongly chaotic single top. However, when a strongly chaotic top is strongly coupled to another such top, $\Delta N_{\rm eff}$ corresponding to any subsystem reaches very close to *unity*. We have again explained this by means of RMT calculations.

Then we studied entanglement production in coupled kicked tops for different underlying classical dynamics of the individual top and also for different coupling strengths. We find, in general, entanglement production is higher for stronger chaotic cases. Moreover, coupling strength between two tops is also an important parameter for the entanglement production. For example, when the coupling strength between two tops is very weak, we find that entanglement production is higher for sufficiently long time corresponding to nonchaotic cases. Finally, we have derived an approximate formula, based on the ideas of RMT, for the entanglement production in coupled strongly chaotic system. This formula is applicable, unlike perturbation theory, to large coupling strengths and is valid for sufficiently long times.

APPENDIX A: DERIVATION OF EQ. (8)

Let us define ladder operators,

$$J_{1\pm}\equiv J_{x_1}\pm J_{y_1},\quad J_{1+}=J_{1-},$$

$$J_{1+}|m_1\rangle=C_{m_1}|m_1+1\rangle\ \text{ and }\ J_{1-}|m_1\rangle=D_{m_1}|m_1-1\rangle, \tag{A1}$$

where C_{m_1} and D_{m_1} are known functions of j and m_1 and $|m_1\rangle$ are the standard angular momentum basis states. We can write $J_{x_1}=(J_{1+}+J_{1-})/2$. Therefore,

$$J'_{x_1}\otimes I_2=\tfrac{1}{2}U_T^\dagger(J_{1+}\otimes I_2)U_T+\tfrac{1}{2}U_T^\dagger(J_{1-}\otimes I_2)U_T, \tag{A2}$$

where the terms present at the right-hand side are the Hermitian conjugate of each other. Therefore, it is sufficient to determine only one term. Here we will calculate the first term explicitly. We have

$$U_T^\dagger(J_{1+}\otimes I_2)=(U_1\otimes U_2)^\dagger U_{12}^{\epsilon\dagger}(J_{1+}\otimes I_2)U_{12}^{\epsilon}(U_1\otimes U_2). \tag{A3}$$

In $|m_1,m_2\rangle$ basis, $U_{12}^{\epsilon\dagger}(J_{1+}\otimes I_2)U_{12}^{\epsilon}$ is

$$\begin{aligned}&\langle m_1,m_2|U_{12}^{\epsilon\dagger}(J_{1+}\otimes I_2)U_{12}^{\epsilon}|n_1,n_2\rangle\\&=\exp\left[i\frac{\epsilon}{j}(m_1-n_1)m_2\right]\langle m_1|J_{1+}|n_1\rangle\delta_{m_2n_2}\\&=\exp\left[i\frac{\epsilon}{j}(m_1-n_1)m_2\right]C_{n_1}\delta_{m_1,n_1+1}\delta_{m_2n_2}\\&=\exp\left[i\frac{\epsilon}{j}m_2\right]C_{n_1}\delta_{m_1,n_1+1}\delta_{m_2n_2}.\end{aligned} \tag{A4}$$

The above expression can also be written as

$$\begin{aligned}&\langle m_1,m_2|U_{12}^{\epsilon\dagger}(J_{1+}\otimes I_2)U_{12}^{\epsilon}|n_1,n_2\rangle\\&=\langle m_1,m_2|J_{1+}\otimes\exp\left(i\frac{\epsilon}{j}J_{z_2}\right)|n_1,n_2\rangle\\&\Rightarrow U_{12}^{\epsilon\dagger}(J_{1+}\otimes I_2)U_{12}^{\epsilon}=J_{1+}\otimes\exp\left(i\frac{\epsilon}{j}J_{z_2}\right).\end{aligned} \tag{A5}$$

Therefore,

$$\begin{aligned}U_T^\dagger(J_{1+}\otimes I_2)U_T&=(U_1\otimes U_2)^\dagger\left[J_{1+}\otimes\exp\left(i\frac{\epsilon}{j}J_{z_2}\right)\right](U_1\otimes U_2)\\&=(U_1^\dagger J_{1+}U_1)\otimes\left[U_2^\dagger\exp\left(i\frac{\epsilon}{j}J_{z_2}\right)U_2\right].\end{aligned} \tag{A6}$$

Now

$$U_1^\dagger J_{1+} U_1 = U_1^{f^\dagger} U_1^{k^\dagger} J_{1+} U_1^k U_1^f$$
$$= U_1^{f^\dagger} J''_{1+} U_1^f, \quad \text{where } J''_{1+} \equiv U_1^{k^\dagger} J_{1+} U_1^k. \tag{A7}$$

In $\{|m_1\rangle\}$ basis, J''_{1+} can be written as

$$\langle m_1|J''_{1+}|n_1\rangle = \langle m_1|U_1^{k^\dagger} J_{1+} U_1^k|n_1\rangle$$
$$= \exp\left[i\frac{k}{2j}(m_1^2 - n_1^2)\right]\langle m_1|J_{1+}|n_1\rangle$$
$$= \exp\left[i\frac{k}{2j}(m_1^2 - n_1^2)\right] C_{n_1}\delta_{m_1,n_1+1}$$
$$= \exp\left[i\frac{k}{j}\left(n_1 + \frac{1}{2}\right)\right] C_{n_1}\delta_{m_1,n_1+1}$$
$$= \langle m_1|J_{1+}\exp\left[i\frac{k}{j}\left(J_{z_1} + \frac{1}{2}\right)\right]|n_1\rangle$$
$$\Rightarrow J''_{1+} = J_{1+}\exp\left[i\frac{k}{j}\left(J_{z_1} + \frac{1}{2}\right)\right]. \tag{A8}$$

Therefore,

$$U_1^\dagger J_{1+} U_1 = U_1^{f^\dagger} J_{1+}\exp\left[i\frac{k}{j}\left(J_{z_1} + \frac{1}{2}\right)\right] U_1^f. \tag{A9}$$

The operator U_1^f is the rotation operator about the y axis with angle $\pi/2$, therefore $U_1^{f^\dagger}(J_{x_1}, J_{y_1}, J_{z_1})U_1^f = (J_{z_1}, J_{y_1}, -J_{x_1})$. Hence we have

$$U_1^\dagger J_{1+} U_1 = (J_{z_1} + iJ_{y_1})\exp\left[i\frac{k}{j}\left(-J_{x_1} + \frac{1}{2}\right)\right]. \tag{A10}$$

Now we will calculate the other term of Eq. (A6), i.e.,

$$U_2^\dagger \exp\left(i\frac{\epsilon}{j}J_{z_2}\right) U_2$$
$$= U_2^{f^\dagger} U_2^{k^\dagger}\exp\left(i\frac{\epsilon}{j}J_{z_2}\right) U_2^k U_2^f$$
$$= U_2^{f^\dagger}\exp\left(i\frac{\epsilon}{j}J_{z_2}\right) U_2^f (\text{since } [U_2^k, J_{z_2}] = 0)$$
$$= \exp\left(-i\frac{\epsilon}{j}J_{x_2}\right)[\text{since } U_2^f \text{ is rotation matrix}]. \tag{A11}$$

Substituting all the above results in Eq. (A6), we get

$$U_T^\dagger(J_{1+}\otimes I_2)U_T = (J_{z_1} + iJ_{y_1})\exp\left[i\frac{k}{j}\left(-J_{x_1} + \frac{1}{2}\right)\right]$$
$$\otimes\exp\left(-i\frac{\epsilon}{j}J_{x_2}\right). \tag{A12}$$

By taking the Hermitian conjugate of the above expression, we determine

$$U_T^\dagger(J_{1-}\otimes I_2)U_T = \exp\left[-i\frac{k}{j}\left(-J_{x_1} + \frac{1}{2}\right)\right](J_{z_1} - iJ_{y_1})$$
$$\otimes\exp\left(i\frac{\epsilon}{j}J_{x_2}\right). \tag{A13}$$

Substituting, last two expressions in Eq. (A2), we will get Eq. (8).

APPENDIX B: CALCULATION OF THE INTEGRAL PRESENT IN EQS. (34) AND (43)

We know $\langle m|z\rangle = \langle m|\theta,\phi\rangle$, and using Eq. (12), the above mentioned integral becomes

$$\frac{2j+1}{4\pi}\sqrt{\binom{2j}{j-i}\binom{2j}{j-k}\binom{2j}{j-l}\binom{2j}{j-m}}$$
$$\times\int_{\theta=0}^{\pi}\int_{\phi=-\pi}^{\pi}\left(1+\tan^2\frac{\theta}{2}\right)^{-4j}\left(\tan\frac{\theta}{2}\right)^{4j-i-k-l-m}$$
$$\times\exp[-i\phi\{(i+l)-(k+m)\}]\sin\theta d\theta d\phi. \tag{B1}$$

After performing the ϕ integral, we get

$$(2j+1)\sqrt{\binom{2j}{j-i}\binom{2j}{j-k}\binom{2j}{j-l}\binom{2j}{j-m}}\delta_{i+l,k+m}$$
$$\times\int_{\theta=0}^{\pi}\left(\cos\frac{\theta}{2}\right)^{4j+2(i+l)+1}\left(\sin\frac{\theta}{2}\right)^{4j-2(i+l)+1}d\theta. \tag{B2}$$

Substituting $\eta = \theta/2$, we get

$$2(2j+1)\sqrt{\binom{2j}{j-i}\binom{2j}{j-k}\binom{2j}{j-l}\binom{2j}{j-m}}\delta_{i+l,k+m}$$
$$\times\int_{\eta=0}^{\pi/2}(\sin\eta)^{4j-2(i+l)+1}(\cos\eta)^{4j+2(i+l)+1}d\eta. \tag{B3}$$

The above integral is a β integral, and therefore we get

$$(2j+1)\sqrt{\binom{2j}{j-i}\binom{2j}{j-k}\binom{2j}{j-l}\binom{2j}{j-m}}\beta[\{(2j+1)$$
$$-(i+l)\},\{(2j+1)+(i+l)\}]\delta_{i+l,k+m}. \tag{B4}$$

From the relation, $\beta(m,n)=[\Gamma(m)\Gamma(n)]/\Gamma(m+n)$, we get

$$\frac{2j+1}{\Gamma(4j+2)}\sqrt{\binom{2j}{j-i}\binom{2j}{j-k}\binom{2j}{j-l}\binom{2j}{j-m}}\,\Gamma\{(2j+1)-(i+l)\}\Gamma\{(2j+1)+(i+l)\}\delta_{i+l,k+m}. \tag{B5}$$

We know that, for any integer m, $\Gamma(m+1)=m!$. Using this relation the above expression will be equal to Eqs. (35) and (44).

APPENDIX C: CALCULATION OF EQ. (62)

Let us first calculate the sum present in the expression of $p(\epsilon)$. That sum can be simplified in the following way:

$$\begin{aligned}\sum_{m_1,m_2=-j}^{+j}\exp\left(-i\frac{\epsilon}{j}m_1m_2\right)&=\frac{2N-1}{N^2}+\frac{1}{N^2}\left[\sum_{m_1=1}^{j}\sum_{m_2=1}^{j}\exp\left(-i\frac{\epsilon}{j}m_1m_2\right)+\sum_{m_1=-j}^{-1}\sum_{m_2=1}^{j}\exp\left(-i\frac{\epsilon}{j}m_1m_2\right)\right.\\&\left.+\sum_{m_1=1}^{j}\sum_{m_2=-j}^{-1}\exp\left(-i\frac{\epsilon}{j}m_1m_2\right)+\sum_{m_1=-j}^{-1}\sum_{m_2=-j}^{-1}\exp\left(-i\frac{\epsilon}{j}m_1m_2\right)\right]\\&=\frac{2N-1}{N^2}+\frac{2}{N^2}\left[\sum_{m_1,m_2=1}^{j}\exp\left(i\frac{\epsilon}{j}m_1m_2\right)+\sum_{m_1,m_2=1}^{j}\exp\left(-i\frac{\epsilon}{j}m_1m_2\right)\right]\\&=\frac{2N-1}{N^2}+\frac{4}{N^2}\mathrm{Re}\sum_{m_1,m_2=1}^{j}\exp\left(i\frac{\epsilon}{j}m_1m_2\right),\end{aligned} \tag{C1}$$

where Re is denoting the real part. Now we define $x\equiv m_1/j$, $y\equiv m_2/j$ and $\delta\equiv 1/j$, where $\delta\to 0$ in large j limit. We can convert the above sum into an integral in the large j limit as

$$j^2\lim_{\delta\to 0}\int_{x=\delta}^{1}\int_{y=\delta}^{1}dx\,dy\cos(j\epsilon xy)=j^2\lim_{\delta\to 0}\int_{x=\delta}^{1}\frac{\sin(j\epsilon x)}{j\epsilon x}dx=\frac{j}{\epsilon}\mathrm{Si}(j\epsilon) \tag{C2}$$

In the large j limit, $N=2j+1\simeq 2j$, therefore

$$p(\epsilon)\simeq\frac{2N-1}{N^2}+\frac{2}{N\epsilon}\mathrm{Si}\left(\frac{N\epsilon}{2}\right). \tag{C3}$$

If we neglect N^{-2} term, then we get

$$p(\epsilon)\simeq\frac{2}{N}\left[1+\frac{\mathrm{Si}\left(\frac{N\epsilon}{2}\right)}{\epsilon}\right]. \tag{C4}$$

Let us now calculate the bigger sum [see Eq. (61)]. If we define $l_1\equiv m_1-n_1$ and $l_2\equiv m_2-n_2$, then this sum will become

$$\begin{aligned}&\sum_{l_1,l_2=-M}^{+M}(N-|l_1|)(N-|l_2|)\exp\left(-i\frac{\epsilon}{j}l_1l_2\right),\quad\text{where } M=2j=N-1,\\&=2N\sum_{l_1=-M}^{+M}(N-|l_1|)+\sum_{\substack{l_1=-M\\l_1\neq 0}}^{+M}\sum_{\substack{l_2=-M\\l_2\neq 0}}^{+M}(N-|l_1|)(N-|l_2|)\exp\left(-i\frac{\epsilon}{j}l_1l_2\right)\\&=4N^2M+4\mathrm{Re}\sum_{l_1,l_2=1}^{M}(N-l_1)(N-l_2)\exp\left(i\frac{\epsilon}{j}l_1l_2\right)\\&=4N^2M+4N^2\mathrm{Re}\sum_{l_1,l_2=1}^{M}\exp\left(i\frac{\epsilon}{j}l_1l_2\right)-8N\mathrm{Re}\sum_{l_1,l_2=1}^{M}l_1\exp\left(i\frac{\epsilon}{j}l_1l_2\right)+4\mathrm{Re}\sum_{l_1,l_2=1}^{M}l_1l_2\exp\left(i\frac{\epsilon}{j}l_1l_2\right).\end{aligned} \tag{C5}$$

We can write the first sum of the above expression as

$$\sum_{l_1,l_2=1}^{M} \exp\left(i\frac{\epsilon}{j} l_1 l_2 \right) = \sum_{l_1,l_2=1}^{M} \exp\left(i\frac{2\epsilon}{M} l_1 l_2 \right). \quad \text{(C6)}$$

This sum is similar to the sum which we have calculated to derive $p(\epsilon)$, see Eq. (C1). Therefore, using this previous result, we get the above sum as

$$\sum_{l_1,l_2=1}^{M} \exp\left(i\frac{\epsilon}{j} l_1 l_2 \right) \simeq \frac{M}{2\epsilon} \mathrm{Si}(2M\epsilon). \quad \text{(C7)}$$

Now

$$\text{Second sum} = \mathrm{Re} \sum_{l_1,l_2=1}^{M} l_1 \exp\left(i\frac{\epsilon}{j} l_1 l_2 \right)$$

$$\simeq M^3 \lim_{\delta\to 0} \int_{x=\delta}^{1}\int_{y=\delta}^{1} x\cos(2M\epsilon xy)\,dx\,dy$$

$$\simeq \frac{M^2}{2\epsilon}\int_0^1 \sin(2M\epsilon x)\,dx \simeq \frac{M}{4\epsilon^2}[1-\cos(2M\epsilon)]. \quad \text{(C8)}$$

$$\text{Third sum} = \mathrm{Re} \sum_{l_1,l_2=1}^{M} l_1 l_2 \exp\left(i\frac{\epsilon}{j} l_1 l_2 \right)$$

$$\simeq M^4 \lim_{\delta\to 0} \int_{x=\delta}^{1}\int_{y=\delta}^{1} dx\,dy\,xy\cos(2M\epsilon xy)$$

$$\simeq \frac{M^3}{2\epsilon}\lim_{\delta\to 0}\left[\int_{x=\delta}^{1} \sin(2M\epsilon x)\,dx + \int_{x=\delta}^{1} \frac{\cos(2M\epsilon x)-1}{2M\epsilon x}\,dx \right]$$

$$\simeq \frac{M^2}{4\epsilon^2}[1-\cos(2M\epsilon)+\mathrm{Ci}(2M\epsilon)-\ln(2M\epsilon)-\gamma]. \quad \text{(C9)}$$

For large j limit, $M \simeq N$ and therefore substituting above results in Eq. (C5), we will arrive at Eq. (62).

[1] E. Schrödinger, Proc. Cambridge Philos. Soc. **31**, 555 (1935).
[2] A. Einstein, B. Podolsky, and N. Rosen, Phys. Rev. **47**, 777 (1935); J.S. Bell, Physics (Long Island City, N.Y.) **1**, 195 (1964).
[3] M. A. Nielsen and I. L. Chuang, *Quantum Computation and Quantum Information* (Cambridge University Press, Cambridge, 2000).
[4] W.H. Zurek, Phys. Rev. D **24**, 1516 (1981); **26**, 1862 (1982); W.H. Zurek, Rev. Mod. Phys. **75**, 715 (2003).
[5] B. Georgeot and D.L. Shepelyansky, Phys. Rev. E **62**, 3504 (2000); **62**, 6366 (2000).
[6] D. Braun, Phys. Rev. A **65**, 042317 (2002)
[7] B. Georgeot and D.L. Shepelyansky, Phys. Rev. Lett. **86**, 2890 (2001).
[8] P.G. Silvestrov, H. Schomerus, and C.W.J. Beenakker, Phys. Rev. Lett. **86**, 5192 (2001).
[9] S. Bettelli and D.L. Shepelyansky, Phys. Rev. A **67**, 054303 (2003).
[10] K. Furuya, M.C. Nemes, and G.Q. Pellegrino, Phys. Rev. Lett. **80**, 5524 (1998).
[11] R.M. Angelo, K. Furuya, M.C. Nemes, and G.Q. Pellegrino, Phys. Rev. E **60**, 5407 (1999).
[12] R.M. Angelo, K. Furuya, M.C. Nemes, and G.Q. Pellegrino, Phys. Rev. A **64**, 043801 (2001).
[13] P.A. Miller and S. Sarkar, Phys. Rev. E **60**, 1542 (1999).
[14] A. Lakshminarayan, Phys. Rev. E **64**, 036207 (2001).
[15] J.N. Bandyopadhyay and A. Lakshminarayan, Phys. Rev. Lett. **89**, 060402 (2002).
[16] A. Tanaka, H. Fujisaki, and T. Miyadera, Phys. Rev. E **66**, 045201(R) (2002); H. Fujisaki, T. Miyadera, and A. Tanaka, *ibid.* **67**, 066201 (2003).
[17] A. Lahiri, e-print quant-ph/0302029v2; A. Lahiri and S. Nag, Phys. Lett. A **318**, 6 (2003).
[18] A.J. Scott and C.M. Caves, J. Phys. A **36**, 9553 (2003).
[19] W.H. Zurek and J.P. Paz, Phys. Rev. Lett. **72**, 2508 (1994); W.H. Zurek and J.P. Paz, Physica D **83**, 300 (1995).
[20] D. Monteoliva and J.P. Paz, Phys. Rev. Lett. **85**, 3373 (2000); Phys. Rev. E **64**, 056238 (2001).
[21] P. Bianucci, J.P. Paz, and M. Saraceno, Phys. Rev. E **65**, 046226 (2002).
[22] A.K. Pattanayak, Phys. Rev. Lett. **83**, 4526 (1999).
[23] P.A. Miller and S. Sarkar, Nonlinearity **12**, 419 (1999); S. Nag, A. Lahiri, and G. Ghosh, Phys. Lett. A **292**, 43 (2001).
[24] A.K. Pattanayak and P. Brumer, Phys. Rev. E **56**, 5174 (1997); Phys. Rev. Lett. **79**, 4131 (1997).
[25] A.K. Pattanayak, B. Sundaram, and B.D. Greenbaum, Phys. Rev. Lett. **90**, 014103 (2003).
[26] H. Kubotani, T. Okamura, and M. Sakagami, Physica A **214**, 560 (1995).
[27] D. Cohen and T. Kottos, e-print cond-mat/0302319.
[28] F. Haake, M. Kus, and R. Scharf, Z. Phys. B **65**, 381 (1987); F. Haake, *Quantum Signatures of Chaos*, 2nd ed. (Springer-Verlag, Berlin, 2000).
[29] G.M. D'Ariano, L.R. Evangelista, and M. Saraceno, Phys. Rev. A **45**, 3646 (1992).
[30] J. J. Sakurai, *Modern Quantum Mechanics* (Addison-Wesley, Reading, MA, 1994).
[31] A. Peres and D. Terno, Phys. Rev. E **53**, 284 (1996).
[32] D. A. Varshalovich, A. N. Moskalev, and V. K. Khersonskii, *Quantum Theory of Angular Momentum* (World Scientific, Singapore, 1988).
[33] A. Wehrl, Rep. Math. Phys. **16**, 353 (1979); A. Wehrl, Rev. Mod. Phys. **50**, 221 (1978).
[34] A. Sugita and H. Aiba, Phys. Rev. E **65**, 036205 (2002).
[35] E.J. Heller, Phys. Rev. A **35**, 1360 (1987).
[36] C. Manderfeld, J. Phys. A **36**, 6379 (2003).